STABILITY OF A 24-BUS POWER SYSTEM WITH CONVERTER INTERFACED GENERATION

A Thesis
Presented to
The Academic Faculty

by

Christopher D. Weldy

In Partial Fulfillment
of the Requirements for the Degree
Master of Science in the
School of Electrical and Computer Engineering

Georgia Institute of Technology
May 2015

STABILITY OF A 24-BUS POWER SYSTEM WITH CONVERTER INTERFACED GENERATION

Approved by:

Dr. A.P. Sakis Meliopoulos, Advisor
School of Electrical and Computer Engineering
Georgia Institute of Technology

Dr. Maryam Saeedifard
School of Electrical and Computer Engineering
Georgia Institute of Technology

Dr. David Taylor
School of Electrical and Computer Engineering
Georgia Institute of Technology

Date Approved: May 2015

To my family

ACKNOWLEDGEMENTS

I would like to thank my advisor Dr. A.P. Meliopoulos for the opportunity to work on this research project, and for his guidance during my time at Georgia Tech. I would also like to thank Dr. Maryam Saeedifard and Dr. David Taylor for serving as committee members. I would like to thank my wife for her persistent encouragement which convinced and enabled me to further pursue education.

TABLE OF CONTENTS

LIST OF TABLES

LIST OF FIGURES

LIST OF SYMBOLS OR ABBREVIATIONS

1LG	Single Phase to Ground Fault.
3LG	Three Phase to Ground Fault.
AC	Alternating Current.
CIG	Converter Interfaced Generation.
DFIG	Doubly Fed Induction Generator.
Hz	Hertz.
L-L	Phase to Phase Fault.
LVRT	Low Voltage Ride Through.
MVAR	Megavolt-Ampere Reactive.
MW	Megawatt.
NREL	National Renewable Energy Laboratory.
PF	Power Factor.
PWM	Pulse Width Modulation.
RTS	IEEE Reliability Test System.
SVC	Static Var Compensator.
TSAT	Transient Security Assessment Tool.
VSC	Voltage Source Converter.
WECC	Western Electricity Coordinating Council.

SUMMARY

The objective of this Masters Thesis is to investigate the system stability implications of integration of power electronic converter interfaced generation (CIG) into conventional power systems. Due to differences between conventional generation and CIG, the power system fault currents, voltage response, and frequency response will likely change with increased penetration of CIG. This research has employed state of the art software tools to perform simulations on the IEEE 24-Bus Reliability Test System (RTS-24), appropriately modified to include converter interfaced generation. Time-domain dynamic simulations and fault calculations have been performed for the system. A comprehensive set of simulations has been performed on the base case, comprised entirely of conventional generation. Conventional generation was replaced by CIG in the model, one generating station at a time until CIG penetration reached one-hundred percent. The comprehensive set of simulations has been performed at each level of CIG penetration. The results have been compared to the base case, with a focus on voltage response, frequency response, and fault current levels of the power system.

As conventional generation is replaced by CIG the system frequency declines to lower and lower minimum values in response to disturbances. Furthermore, the system voltages oscillate at higher and higher frequencies and can resolve at undesirable deviations from their initial values. These undesirable results, however, can be mitigated by active and reactive power injections in response to system disturbances. To mitigate some of the issues observed in the maximum CIG power system, active and reactive power injections were modeled to represent the potential contribution to dynamic stability of the system. Use of active power injection in response to a

fault is shown to mitigate some of the additional frequency dip caused by reduction in generator inertia. Use of reactive power injection in response to a fault is shown to mitigate some of the voltage deviation observed due to insufficient reactive power margin of available generation.

Power electronic converter rating limits have a significant impact on fault current levels in the system, but the network impedance is shown to reduce the impact of these converter limitations at locations remote from the converter. As penetration of CIG into the power system increases, fault current levels begin to approach load current levels in proximity to the converters. This condition in large-scale power systems may require new protection methods to maintain reliable and secure protection as power systems evolve.

CHAPTER 1

INTRODUCTION

Power systems around the world are seeing consistent increase of CIG capacity, which is largely due to increases in renewable energy generation connected to power systems through power electronic converters. For example, installed wind power capacity worldwide increased by a factor of ten between the end of 2000 and the end of 2010[1]. The characteristics of power electronic converters are very different than conventional source equipment connected to the power system. Power electronic limitations, CIG control modes, and decoupling of mechanical inertia are differences expected to cause significant impact to the stability of the power system.

Because of strict limitations of power electronic equipment, fault currents contributed by CIG can be significantly lower than those contributed by conventional generators. These limitations lead to fault currents that can be difficult to distinguish from maximum load currents. This makes reliable and secure protection of the power system difficult to achieve. Additionally, CIG offers control modes not available to conventional generation and CIG response times are based on electrical time constants, which are typically much shorter than the mechanical time constants of conventional generators. CIG control modes, coupled with shorter time constants will likely have an impact on the voltage response of the power system. Finally, CIG does not couple mechanical inertia to the power system directly, like conventional generation. The mechanical inertia provided to the power system by conventional generation plays an important role in maintaining system frequency during disturbances. Since CIG does not have inertia available to help maintain the system frequency during disturbances, power systems with a high penetration of CIG will likely have different

frequency response characteristics than conventional power systems. This research has investigated the system changes due to integration of CIG into a generic conventional power system. Fault current levels, voltage response, and frequency response have been compared for the power system at increasing levels of CIG integration.

CHAPTER 2

BACKGROUND AND LITERATURE REVIEW

This chapter summarizes some important fundamental concepts. Power flow, fault analysis, and dynamic stability of power systems are reviewed. General descriptions of power system equipment will be given.

2.1 Basic Concepts

Power systems cover large geographic areas and are subject to a variety of weather conditions, among other adversities. Because of this, power systems are regularly subject to disturbances. It is desirable to know in advance whether a power system will be able to survive all reasonable disturbances that may occur, and to assess whether operational actions may be necessary. In order to study this, models are developed for the power system and disturbances are simulated to determine the system response. Simulation of a power system using models typically involves the solution of a variety of large scale numerical problems. For each disturbance, the power system response is studied to identify and categorize undesirable behavior. Voltage stability, rotor angle stability, and frequency stability are of primary interest in this research. Although the various forms of stability are distinguished, they are often coupled to one another and occur together.

2.1.1 Simulation

Due to the tremendous cost of power systems it is usually impractical to physically build a test system. Therefore, it is common practice to develop mathematical models of power systems, upon which simulations can be performed. In some cases, the simulations can be compared to sampled data from existing power systems to verify the

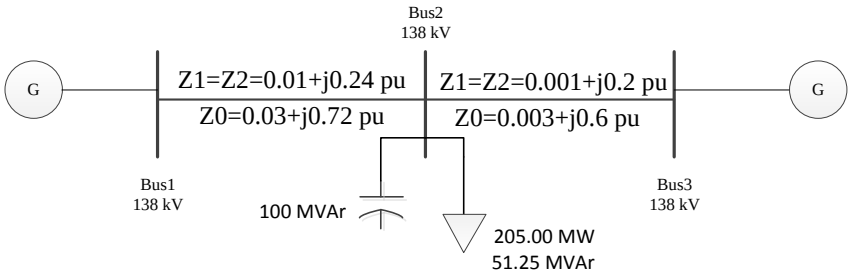

Figure 1: Test System Oneline Diagram

accuracy of results. Modeling and simulation of conventional power systems is fairly mature, being one of the early tasks for computers. However, as power system equipment evolves and new devices are created, new models and solution techniques are needed to accurately portray the power system using simulations. This research uses commercially available simulation software and models. The conventional equipment models are fairly mature, while the CIG equipment models are relatively new.

2.1.2 Simple Demonstration System

Figure 1 shows a oneline diagram of a simple power system which will be used to review the relevant concepts of power system analysis. This power system is comprised of one electrical load fed by two sources through transmission lines. The generator connected to Bus1 is large compared to the generator connected to Bus3. The system is modeled at 138 kV on a 100 MVA base. The dynamic model parameters for this test system are shown in Tables 1, 2, 3, and 4.

2.1.3 Power Flow Analysis

Power flow analysis consists of solving the network equations representing a power system, to identify the active and reactive power flowing in each part of the system. The following equations are used to obtain network equations for a given power

Table 1: GENROU Model Parameters for the Simple System Rotors

	Bus1	Bus3
T'do	7.5	7.5
T"do	0.054	0.054
T'qo	1.5	1.5
T"qo	0.107	0.107
H	11.4	11.4
D	0	0
Xd	1.64	1.64
Xq	1.575	1.575
X'd	0.159	0.159
X'q	0.306	0.306
X"d	0.102	0.102
Xl	0.113	0.113
S(1.0)	0.087	0.087
S(1.2)	0.2681	0.2681
MVA Base	1000	25

Table 2: ESAC1A Model Parameters for the Simple System Excitation Systems

	Bus1	Bus3
TR	0	0
TB	0	0
TC	0	0
KA	400	400
TA	0.02	0.02
VAMAX	14.5	14.5
VAMIN	-14.5	-14.5
TE	0.8	0.8
KF	0.03	0.03
TF	1	1
KC	0.2	0.2
KD	0.38	0.38
KE	1	1
E1	4.18	4.18
SE(E1)	0.1	0.1
E2	3.14	3.14
SE(E2)	0.03	0.03
VRMAX	6.03	6.03
VRMIN	-5.43	-5.43
MVA Base	1000	25

Table 3: IEESGO Model Parameters for the Simple System Governor Systems

	Bus1	Bus3
T1	0.5	0.5
T2	1.25	1.25
T3	0.7	0.7
T4	0.7	0.7
T5	0	0
T6	0	0
K1	25	25
K2	0	0
K3	0	0
PMAX	1	1
PMIN	0	0
MVA Base	1000	25
Pgen (Powerflow)	183.4962	25
Pmax (Powerflow)	999	999

Table 4: CLODAR Model Parameters for the Simple System Dynamic Loads

IAREA	1
Area	Area1
LMpct	30
SMpct	30
TEXpct	2
DISpct	8
MVApct	30
KP	1
R	0
X	0

system[2].

$$P_{ik}(x) = \sum_{k=1}^{n} |V_i||V_k|\big(g_{ik}cos\left(\delta_i - \delta_k\right) + b_{ik}sin\left(\delta_i - \delta_k\right)\big) \tag{1}$$

$$Q_{ik}(x) = \sum_{k=1}^{n} |V_i||V_k|\big(g_{ik}sin\left(\delta_i - \delta_k\right) - b_{ik}cos\left(\delta_i - \delta_k\right)\big) \tag{2}$$

In order to find the correct parameters for these equations, an admittance matrix of the following form is typically obtained.

$$Y_{bus} = \begin{bmatrix} Y_{11} & \dots & Y_{1n} \\ \vdots & \ddots & \vdots \\ Y_{n1} & \dots & Y_{nn} \end{bmatrix} \tag{3}$$

Once the equations for a system are identified, one of many numerical methods can be used to solve the set of non-linear equations[3]. For example, the following is a representation of the Newton-Rhapson method, which is commonly used to solve the power flow problem.

$$\begin{bmatrix} x_1^{n+1} \\ \vdots \\ x_n^{n+1} \end{bmatrix} = \begin{bmatrix} x_1^{n} \\ \vdots \\ x_n^{n} \end{bmatrix} - \begin{bmatrix} \frac{\partial g_1}{\partial x_1} & \dots & \frac{\partial g_1}{\partial x_n} \\ \vdots & \ddots & \vdots \\ \frac{\partial g_n}{\partial x_1} & \dots & \frac{\partial g_n}{\partial x_n} \end{bmatrix}^{-1} \cdot \begin{bmatrix} g_1(x_1^n, \dots, x_n^n) \\ \vdots \\ g_n(x_1^n, \dots, x_n^n) \end{bmatrix} \tag{4}$$

Table 5 shows three iterations of the Newton-Rhapson method when applied to solve the simple system shown in Figure 1. These iterations were calculated using a Python script which is documented in Appendix B for reference. The final result

Table 5: Newton-Rhapson Iterations for Simple System

Iteration	δ_2	δ_3	V_2
0	0	0	1
1	-24.9	-22.02	1.045
2	-25.84	-22.98	1.001
3	-25.95	-23.08	0.9984

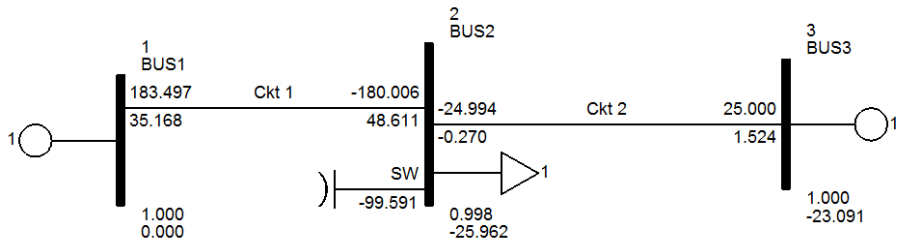

Figure 2: Commercial Software Power Flow Solution

is in agreement with the result obtained using the commercial power flow analysis software shown in Figure 2.

Solution of the power flow problem is important in this research, because this solution provides the initial conditions for a dynamic simulation, which is discussed later.

2.1.4 Fault Analysis

Fault analysis of the power systems can be performed using the method of symmetrical components[2][4][5]. The method of symmetrical components involves transforming three phase quantities into three distinct balanced sets of components, two of which are balanced and one which is a set of three identical quantities. Figure 3 shows the symmetrical component model of the test system. Notice that the load is neglected in the diagram, since loads are typically neglected in fault studies. The voltage sources in the top circuit are assumed to have 1 per unit voltage throughout the analysis, therefore in the case of balanced operation, no fault current flows in the network. The middle network in Figure 3 represents negative sequence while the lower negative represents zero sequence. Fault analysis can be performed by applying

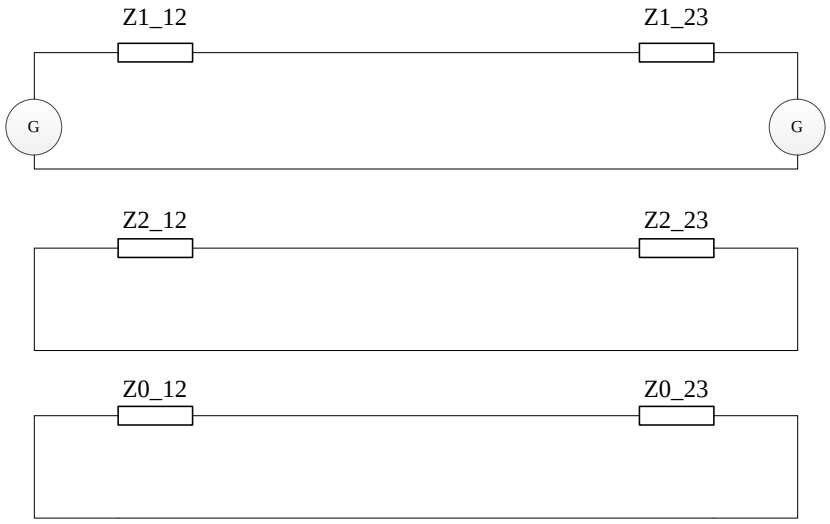

Figure 3: Test System Symmetrical Component Diagram

a fault connection model at the faulted point in the network model and performing circuit analysis. Once the symmetrical component quantities are known, the inverse symmetrical component transform can be used to find the phase quantities. Analysis using this method for a 3LG, a L-L, and a 1LG fault on the test system are provided to demonstrate the general method of fault analysis used in this research.

2.1.4.1 Three Phase Fault

The network diagram used to calculate quantities for a 3LG fault on Bus2 is shown in Figure 4. This diagram shows the complete network with the fault connection model added, and network reduction steps taken to simplify the analysis. Notice that the negative and zero sequence networks are neglected because this analysis assumes a perfectly balanced 3LG fault. The resulting positive sequence current is calculated from the reduced circuit to be $9.16\angle -88.76°pu$.

$$I_1 = \frac{1}{Z_{eq}} = \frac{1}{\frac{1}{\frac{1}{Z1_{12}}+\frac{1}{Z1_{23}}}} = 9.16\angle -88.76°pu \tag{5}$$

The phase currents are calculated by applying the transformation shown in the

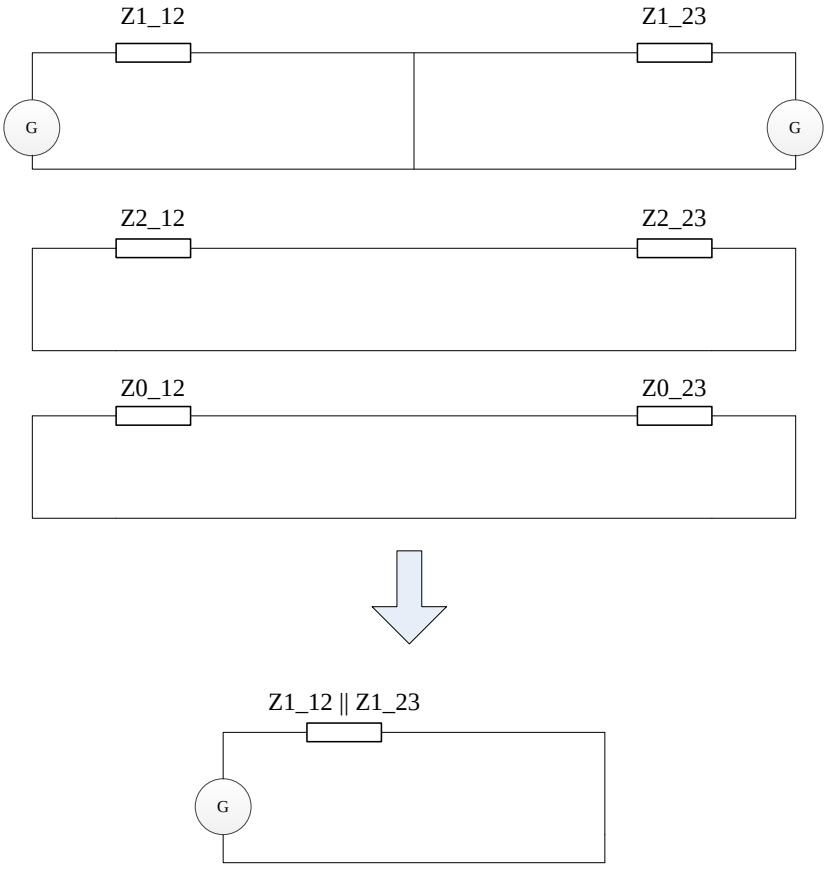

Figure 4: Test System Three Phase Fault

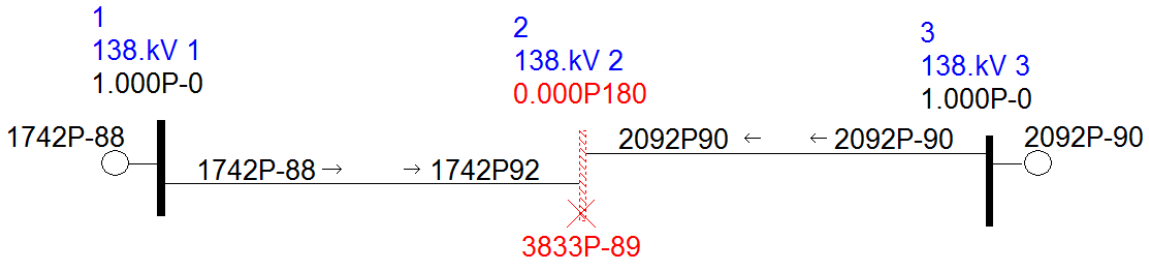

Figure 5: Commercial Software Three Phase Fault

following equation[2][6].

$$\begin{bmatrix} I_A \\ I_B \\ I_C \end{bmatrix} = \begin{bmatrix} 1 & 1 & 1 \\ 1 & 1\angle -120 & 1\angle 120 \\ 1 & 1\angle 120 & 1\angle -120 \end{bmatrix} \cdot \begin{bmatrix} I_0 \\ I_1 \\ I_2 \end{bmatrix} \tag{6}$$

For the 3LG fault on this test system, the resulting currents are shown below in per unit.

$$\begin{bmatrix} I_A \\ I_B \\ I_C \end{bmatrix} = \begin{bmatrix} 1 & 1 & 1 \\ 1 & 1\angle -120 & 1\angle 120 \\ 1 & 1\angle 120 & 1\angle -120 \end{bmatrix} \cdot \begin{bmatrix} 0 \\ 9.16\angle -88.76^\circ \\ 0 \end{bmatrix} = \begin{bmatrix} 9.16\angle -88.76^\circ \\ 9.16\angle 151.24^\circ \\ 9.16\angle 31.24^\circ \end{bmatrix} \tag{7}$$

Notice that the phase fault currents form a balanced set for this balanced 3LG fault. The per unit current is converted into amps by multiplying it by the per unit current base calculated in the following equation.

$$I_{base} = \frac{S_{base}}{\sqrt{3} * V_{base}} = \frac{100MVA}{\sqrt{3} * 138kV} = 418.37\Omega \tag{8}$$

The magnitude of the fault current at Bus2 for a 3LG fault is 3832.88 amps, which is in agreement with the result obtained using the commercial fault analysis software shown in Figure 5.

2.1.4.2 Phase to Phase Fault

The network diagram used to calculate quantities for a L-L fault between phase B and phase C on Bus2 is shown in Figure 6. This diagram shows the complete network with

the fault connection model added, and network reduction steps taken to simplify the analysis. Notice that the zero sequence network is neglected because this network is isolated from all sources for a L-L fault. The resulting positive and negative sequence currents are calculated from the reduced circuit to be $4.58\angle -88.76°$ per unit and $4.58\angle 91.24°$ per unit, respectively.

$$I_1 = \frac{1}{Z_{eq}} = \frac{1}{0.22\angle 88.76°} = 4.58\angle -88.76° pu \tag{9}$$

$$I_2 = \frac{1}{Z_{eq}} = -\frac{1}{0.22\angle 88.76°} = 4.58\angle 91.24° pu \tag{10}$$

The phase currents are calculated using the transformation as before. For the L-L fault on this test system, the resulting currents are shown below in per unit.

$$\begin{bmatrix} I_A \\ I_B \\ I_C \end{bmatrix} = \begin{bmatrix} 1 & 1 & 1 \\ 1 & 1\angle -120 & 1\angle 120 \\ 1 & 1\angle 120 & 1\angle -120 \end{bmatrix} \cdot \begin{bmatrix} 0 \\ 4.58\angle -88.76° \\ 4.58\angle 91.24° \end{bmatrix} = \begin{bmatrix} 0 \\ 7.93\angle -178.76° \\ 7.93\angle 1.24° \end{bmatrix} \tag{11}$$

Notice that the phase B and phase C fault currents are equal in magnitude, but opposite in phase for this L-L fault. The per unit current is converted into amps by multiplying it by the per unit current base calculated previously. The magnitude of the fault current at Bus2 for a L-L fault is 3319.37 amps, which is in agreement with the result obtained using the commercial fault analysis software shown in Figure 7.

2.1.4.3 Single Phase Fault

The network diagram used to calculate quantities for a 1LG fault on phase A at Bus2 is shown in Figure 8. This diagram shows the complete network with the fault connection model added, and network reduction steps taken to simplify the analysis. Notice that positive sequence, negative sequence, and zero sequence networks must all be considered for a 1LG fault. The resulting positive, negative, and zero sequence currents are calculated from the reduced circuit to be $1.83\angle -88.76°$ per unit.

$$I_1 = I_2 = I_0 = \frac{1}{Z_{eq}} = \frac{1}{0.22\angle 88.76°} = 4.58\angle -88.76° pu \tag{12}$$

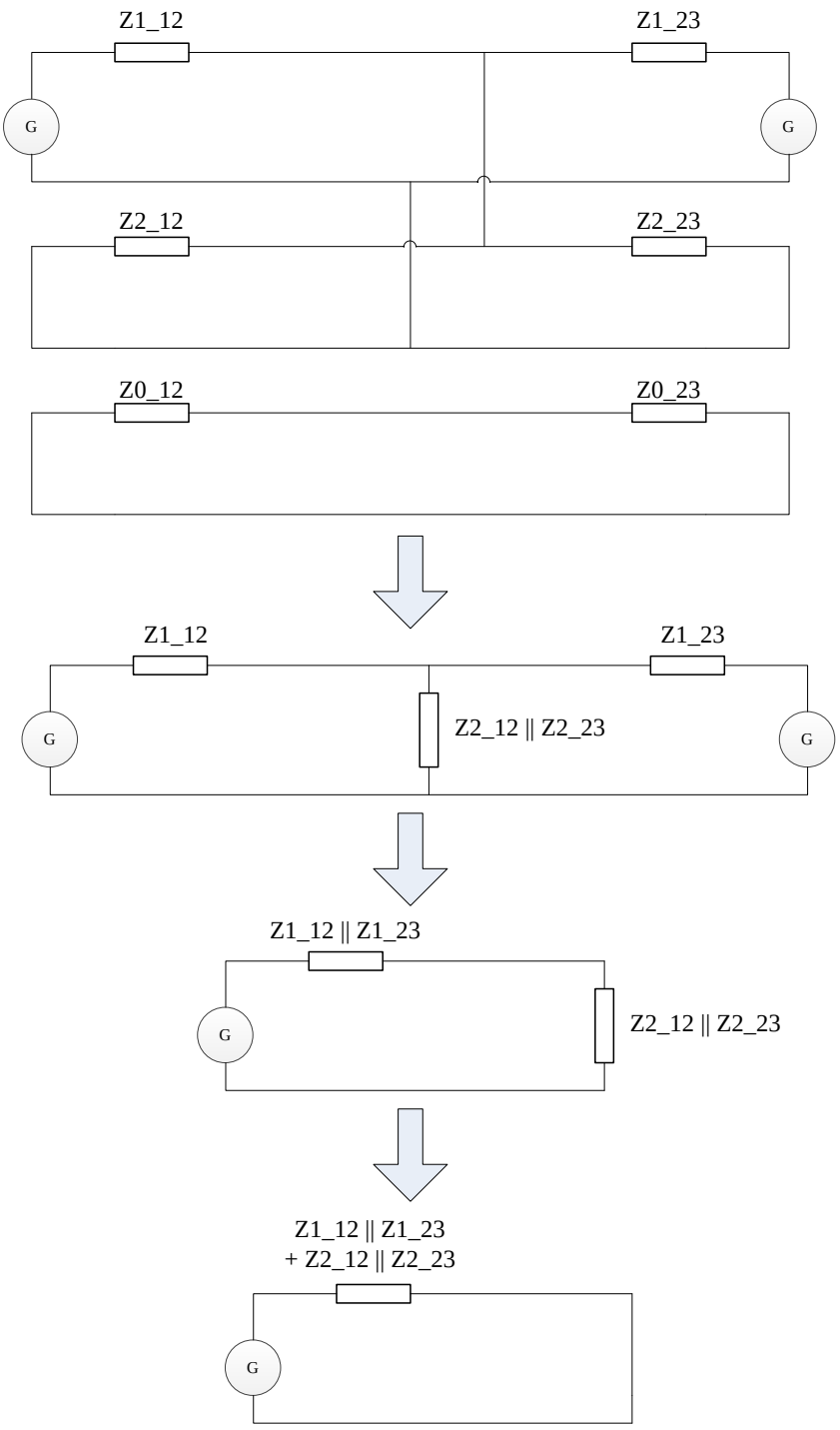

Figure 6: Test System Phase to Phase Fault

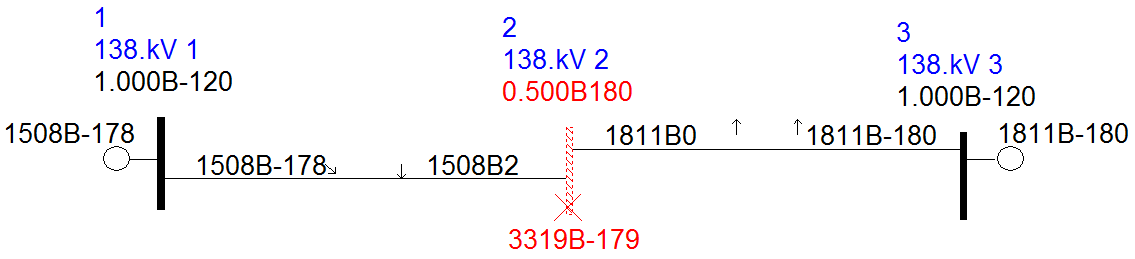

Figure 7: Commercial Software Phase to Phase Fault

The phase currents are calculated using the transformation as before. For the 1LG fault on this test system, the resulting currents are shown below in per unit.

$$\begin{bmatrix} I_A \\ I_B \\ I_C \end{bmatrix} = \begin{bmatrix} 1 & 1 & 1 \\ 1 & 1\angle -120 & 1\angle 120 \\ 1 & 1\angle 120 & 1\angle -120 \end{bmatrix} \cdot \begin{bmatrix} 1.83\angle -88.76° \\ 1.83\angle -88.76° \\ 1.83\angle -88.76° \end{bmatrix} = \begin{bmatrix} 5.50\angle -88.76° \\ 0 \\ 0 \end{bmatrix} \tag{13}$$

Notice that only phase A has fault current for this 1LG fault. The per unit current is converted into amps by multiplying it by the per unit current base calculated previously. The magnitude of the fault current at Bus2 for a 1LG fault is 2299.73 amps, which is in agreement with the result obtained using the commercial fault analysis software shown in Figure 9.

2.1.5 Stability Analysis

Power system stability analysis involves the solution of simultaneous non-linear differential equations and algebraic equations, which mathematically represent the power system network and equipment. The general form is outlined in the following equations, where x is the state vector of the system, V is the bus voltage vector, and I is the current injection vector[7].

$$\dot{x} = f(x, V) \tag{14}$$

$$I(x, V) = Y_N V \tag{15}$$

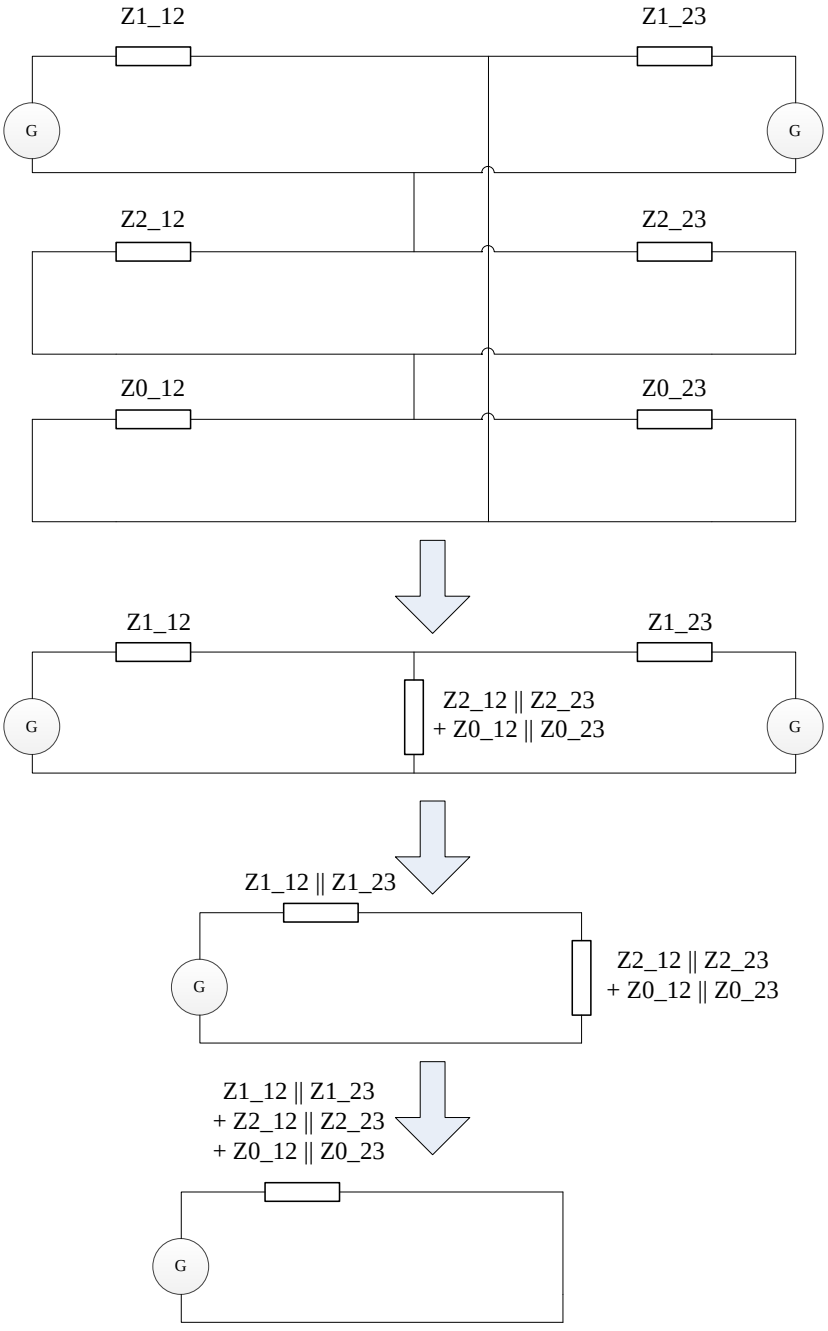

Figure 8: Test System Single Phase Fault

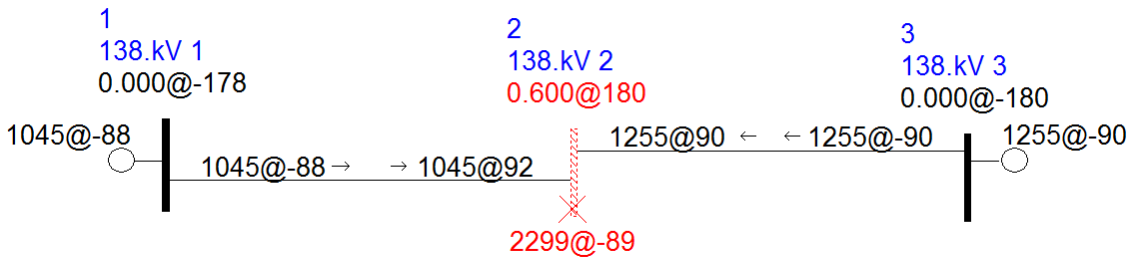

Figure 9: Commercial Software Single Phase Fault

When a power system is modeled in simulation software, the software interprets the system and casts it into this form. Numerical methods are then applied to solve the simultaneous set of equations at each time step. The result is a time-domain response of the power system for a given sequence of events. Solution of this problem is covered in detail by Kundur[7]. The following sections summarize the key concepts of power system stability relating to this research.

2.1.5.1 Voltage Stability

Voltage stability is achieved for a power system when reactive power demand is met by reactive power supply[8]. Voltage instability (or collapse) occurs when reactive power demand exceeds reactive power supply[9], due to insufficient system reactive capacity or due to reactive power transfer constraint caused by network limitations. Dynamic behavior of power system loads, especially electric motors, can have a significant impact on voltage stability. When the supply voltage is depressed for a sufficient duration, the slip of an induction motor increases due to reduced electrical torque. This reduction in electrical torque and speed can lead to motor stalling if the available electrical torque, including torque converted from inertial energy, is less than the load torque. During stall the reactive power absorbed by an induction motor increases significantly, which further increases voltage drops in the network. In severe cases, this behavior can cascade to other parts of the power system.

Figure 10 shows an example of voltage collapse following a disturbance. The

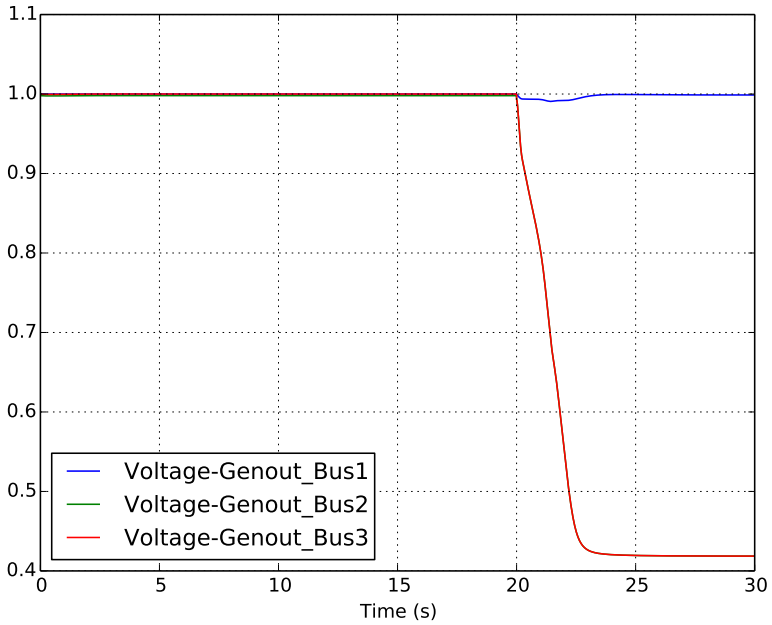

Figure 10: Voltage collapse following generator outage

disturbance was modeled as an outage of generator 2 initiated at 20 seconds. It can be seen that the voltages at Bus2 and Bus3 collapse to unacceptably low values because of the generator outage. Even though Bus1 is able to recover to a voltage of 1.0 per unit, the network constrains reactive power transfer enough to prevent voltage recovery.

2.1.5.2 Rotor Angle Stability

Rotor angle stability is achieved for a power system when generation matches active power demand and oscillations are small and decaying. Instability occurs when oscillations are large to the point that generation and load lose synchronism with each other[9]. Without swift corrective control action, the oscillations can potentially lead to collapse and long term outages of large portions of the power system.

Figure 11 shows an example of rotor angle instability following a disturbance. The disturbance was modeled as a 47 cycle 3LG fault on Bus 3, initiated at 20 seconds. It can be seen that the generator at Bus3 loses synchronism with the system because

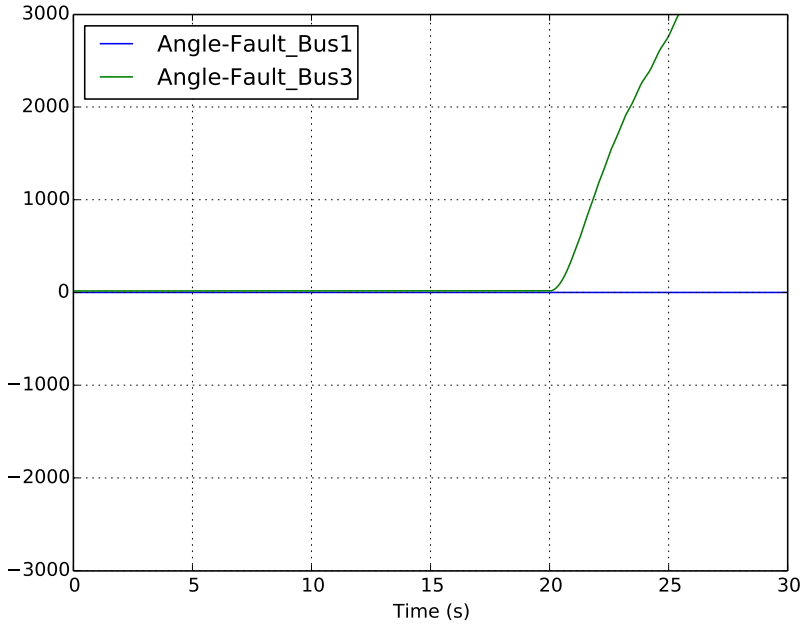

Figure 11: Rotor angle instability following delayed-clearance of fault

of the fault. The simulation did not trip the generator after it lost synchronism, but it reality a generator should be tripped by local protection for this condition. Consequently, this would have led to voltage collapse for this simple power system, as seen in the previous section. The consequences of failure to trip the unit would be severe, and could cause additional issues.

2.1.5.3 Frequency Stability

Frequency stability is achieved for a power system when frequency deviations are small enough that tripping of generation or load is not required. Frequency instability occurs when frequency deviations lead to tripping of enough equipment that unsustainable imbalance between generation and load is developed[9].

Figure 12 shows examples of frequency response following various disturbances. It clearly shows that frequency deviations can be small for a slight reduction in generation, or quite large for faults and generator outages. The response in this case is slightly exaggerated due to the relatively small size of the test system. Frequency

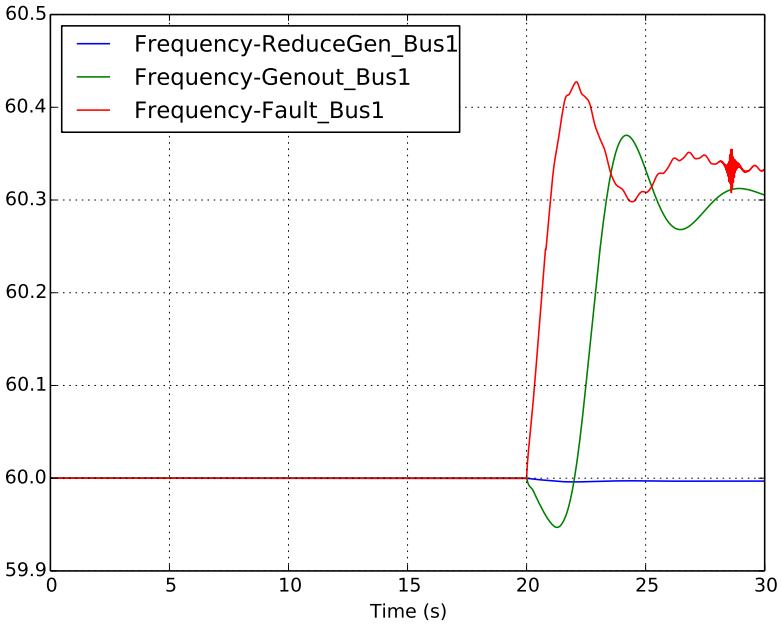

Figure 12: Frequency response for various disturbances

deviations as large as these would be severe on a large scale power system.

Conventional generators couple mechanical inertia to the power system, which is effectively energy storage. During system disturbances the energy stored as inertia can be readily converted into active power at the cost of a reduction in system frequency. The large amount of generation inertia in conventional power systems allows power system needs during disturbances to be met with fairly small deviations in system frequency. Since high penetration CIG systems have less generator inertia, remaining conventional generators must reduce speed significantly to convert the necessary active power. This leads to system frequency dips which can be considerably greater than would be seen in conventional power systems. Frequency nadir, or the lowest frequency, can be used to assess system frequency margin[10].

For the purposes of this research, very slow acting components of the generation were not modeled. Therefore, no equipment is tripped from the power system during simulations due to frequency deviations. Instead, the system frequency was observed

to provide a basis for qualitatively assessing the frequency stability implications of CIG integration.

2.2 Practical Considerations

Due to long service life of power system equipment, it is desirable to understand the characteristics of power systems with high CIG penetration as early as possible. Power system equipment costs are typically measured in millions of dollars, so it is desirable that any equipment last as long as possible. Any information regarding the future of power systems can be very valuable if available early enough. This research aims to contribute to growing efforts in this regard.

The key difference between the proposed research and research already completed is that the proposed research will focus on the technical aspects of a complete conventional power system as it evolves into a complete CIG power system. The proposed research will assume that adequate capacity of variable generation is installed, without delving into weather forecasts, energy availability, or institutional aspects of the power system. That is not to say that these aspects are unimportant, rather they are critically important to the power system as a whole. However, the proposed research will be focused on the stability requirements of a generic power system, assuming that the available generation is capable of supplying the load demand in steady state operation.

The proposed research will utilize the standard public generic models developed for Type IV Wind Machine CIG along with General Electric (GE) parameters which are available for these models. Dynamic simulations will be performed using DSA Tools analysis software, and fault analysis will be performed using ASPEN analysis software.

2.2.1 Equipment

A utility scale power system is comprised of electrical, mechanical, and electromechanical components combined into a cohesive system with the purpose of efficiently and reliably providing electrical power to a set of loads that are geographically and characteristically diverse. The major components which are modeled and discussed in this research include generators, transformers, transmission lines, loads, and power electronic devices. There are other types of devices found in a power system and, being less relevant to this research, are left to the literature.

Generators are sources of electrical energy for the power system. They convert energy from various forms into electrical energy with specific electrical characteristics. The term generator is typically used to describe the entire process of energy conversion and coupling to the power system, which is a very complex control system. The behavior of power systems is largely dependent on the generators, including control parameters and protection.

Loads consist of all equipment that utilize electric power from the power system. Motors, heaters, lighting, and electronic devices are among the most common loads. Loads are connected and disconnected from the power system at times which are largely unpredictable. Patterns can be deduced, but many assumptions must be made when modeling loads, more so than for other equipment. It is common to study a power system at a maximum and a minimum load level to ascertain a range of likely behavior for the system.

The cost of power system equipment typically goes up when voltage goes up, so it is desirable for generators and loads to be connected at relatively low voltages. However, the losses due to transmitting power go up as voltage goes down, so it is desirable to transmit power at very high voltages. Therefore, transformers are used to transfer power between portions of a power system at different voltage levels. Step-up transformers are connected to a generator's low voltage bus and transform the power

to a higher voltage for transmission over long distances. Step-down transformers are connected to high voltage transmission buses and transform the power to a lower voltage for distribution to loads. It is no surprise that power transformers are very expensive, but the cost savings due to low voltage generators and loads substantially compensate for the high cost of transformers. Transformers have significantly high inductive impedances and can be a limiting factor for certain phenomena in the power system, such as fault current magnitudes.

Transmission lines transmit the electrical power through the power system. They are comprised of conductors, towers, earth, and other supporting equipment in various configurations. Transmission lines have resistance, inductance, and capacitance. The impedance of transmission lines can be very small or very large, depending on many factors including conductors, geometry, length, and ratings. Ultimately, any phenomena in the power system is transmitted through the transmission lines, so the characteristics are very important to the overall behavior of a power system.

This research is concerned with the integration of power electronic devices into the transmission system. Although converter interfaced loads can offer tremendous advantages[11] and are becoming more common, the focus here is power electronic sources to the system. CIG uses a power electronic converter to connect to the power system, which acts as a source of active and reactive power. A converter is comprised of solid-state switches which are controlled to transfer power from the generator to the power system, with specifically dictated characteristics. Power electronic converters have very strict limitations, which may introduce new issues into power systems. Furthermore, the behavior of power electronic converters is complicated by protection and control functions which require very detailed models and consideration.

2.3 Existing and Ongoing Research

Research in power systems has contributed and continues to contribute to this vital technology. In recent decades, power electronics technology has enabled practical integration of renewable energy sources to the grid in large quantities. The power electronic converters used to connect renewable sources commonly transfer energy to the grid using some form of pulse width modulation (PWM) control[12], and thus have characteristics which are very different than conventional generation. Furthermore, renewable energy sources are not typically configured to offer the flexibility of dispatchable power, which can complicate system response to disturbances. Because of these issues, and others, research is going on in this area to identify in advance potential problems and needs for power systems with high penetration of CIG. A brief summary of some research in this area is provided.

Displacement of conventional generation with non-dispatchable resources has received a lot of attention. Wind generators connected directly to the power system contribute inertia during disturbance recovery, but their consumption of reactive power can reduce the voltage stability margins[13]. However, reactive compensation can be used in tandem with CIG[14], or the existing converter can be used to provide dynamic reactive support. Although studies indicate that low penetration of wind may benefit the system, high penetration of wind can result in reduction in stability margins[15]. Control modes used for wind generation can impact the stability of conventional generation, and displacement of conventional generation by non-dispatachable resources can lead to loss of system mitigation capabilities[16]. Voltage control modes for Doubly fed induction generators (DFIG) increase system security and improve system voltage response compared to power factor (PF) control, but a system tends to be more stable when more conventional generation is online[17]. As new technologies emerge, new ideas on addressing these issues have been proposed and studied. Emulated inertial response in converters can help alleviate conventional generation

displacement issues[18], although a portion of available resources must be sacrificed.

As CIG increase in a power system, the protection of the grid must be adapted. Although DFIG reduce system inertia when used to displace conventional generation, they can provide sustained short circuit currents during grid faults[19]. This helps enable the use of conventional protection methods for the local grid facilities. In order to prevent issues caused by generation disconnect during disturbances, low voltage ride through (LVRT) requirements are being implemented. This means that the generators are not allowed to disconnect due voltage response within a certain window. LVRT are shown to improve system performance with high penetration of wind[20], so justifying the requirements. Multiple control techniques are available which can help renewable resources meet LVRT requirements[21]. For example, by controlling the converter, DFIG is capable of meeting the LVRT requirements[22]. Issues still exist though, as weak alternating current (AC) system connection can reduce performance of voltage source converters (VSC)[23].

CIG integration into power systems is being investigated by a number of researchers in industry and academia. EPRI, NREL, WECC, and others have collaborated to develop CIG models that are standard, public, and not specific to any vendor. The models are designed to emulate the dynamic behavior of CIG equipment at the terminals of interconnection with the power system. NREL has performed research to determine appropriate capacity factors based on availability of energy sources. NREL has also performed research to assess the needs of systems with increased variable generation, taking into consideration the institutional aspects of the system. Utilities and consulting firms perform interconnection studies for each CIG plant that is connected to specific power systems. Tremendous work has been performed by software vendors to create software interfaces and algorithms which can accommodate CIG models in conventional power system simulation software. Following the lead of EPRI, NREL, and WECC, most large scale CIG manufactures

have performed studies to determine appropriate model parameters to model their equipment using the generic models.

This research aims to contribute to the growing body of research in this area. This research has employed state of the art software tools to perform simulations on the IEEE 24-Bus Reliability Test System (RTS-24), appropriately modified to include converter interfaced generation. Time-domain dynamic simulations and fault calculations have been performed for the system. A comprehensive set of simulations has been performed on the base case, comprised entirely of conventional generation. Conventional generation has been replaced by CIG in the model, one generating station at a time until CIG penetration is one-hundred percent. The comprehensive set of simulations has been performed at each level of CIG penetration. The results have been compared to the base case, with a focus on voltage response, frequency response, and fault current levels of the power system.

CHAPTER 3

24 BUS POWER SYSTEM MODEL

Models are used in this research to simulate the behavior of conventional and CIG power systems. This chapter details the development of eleven power system models prepared for use in steady-state, dynamic, and fault simulations. The IEEE 24-Bus Reliability Test System (RTS)[24] forms the positive sequence base in steady-state. Dynamic equipment models were added to represent generators and loads in the system. Negative and zero sequence networks were added to enable unbalanced fault analysis.

3.1 Conventional Power System

3.1.1 Power Flow Model

The power flow model is a positive sequence representation of the power system and forms the foundation of the dynamic and fault analysis models. This model aims to represent a small but complete power system under steady state conditions where generation and load are well balanced. A power flow model provides a snapshot of voltage magnitudes and angles at buses across the system for a particular operating condition, from which active and reactive power flows can be discerned.

A oneline diagram of the RTS power system is shown in Figure 13. It is comprised of 10 generating plants, 17 load serving points, 5 transformers, and 33 transmission lines. Not shown in the diagram are generation plant step-up transformers, but one is modeled for each plant. The loads were scaled down 10% from the original RTS system and the generation was redispatched to create more margin for disturbance response, since the original model was not intended for dynamic analysis. The system is comprised of transmission facilities at 230 kV and 138 kV. Total load for the system

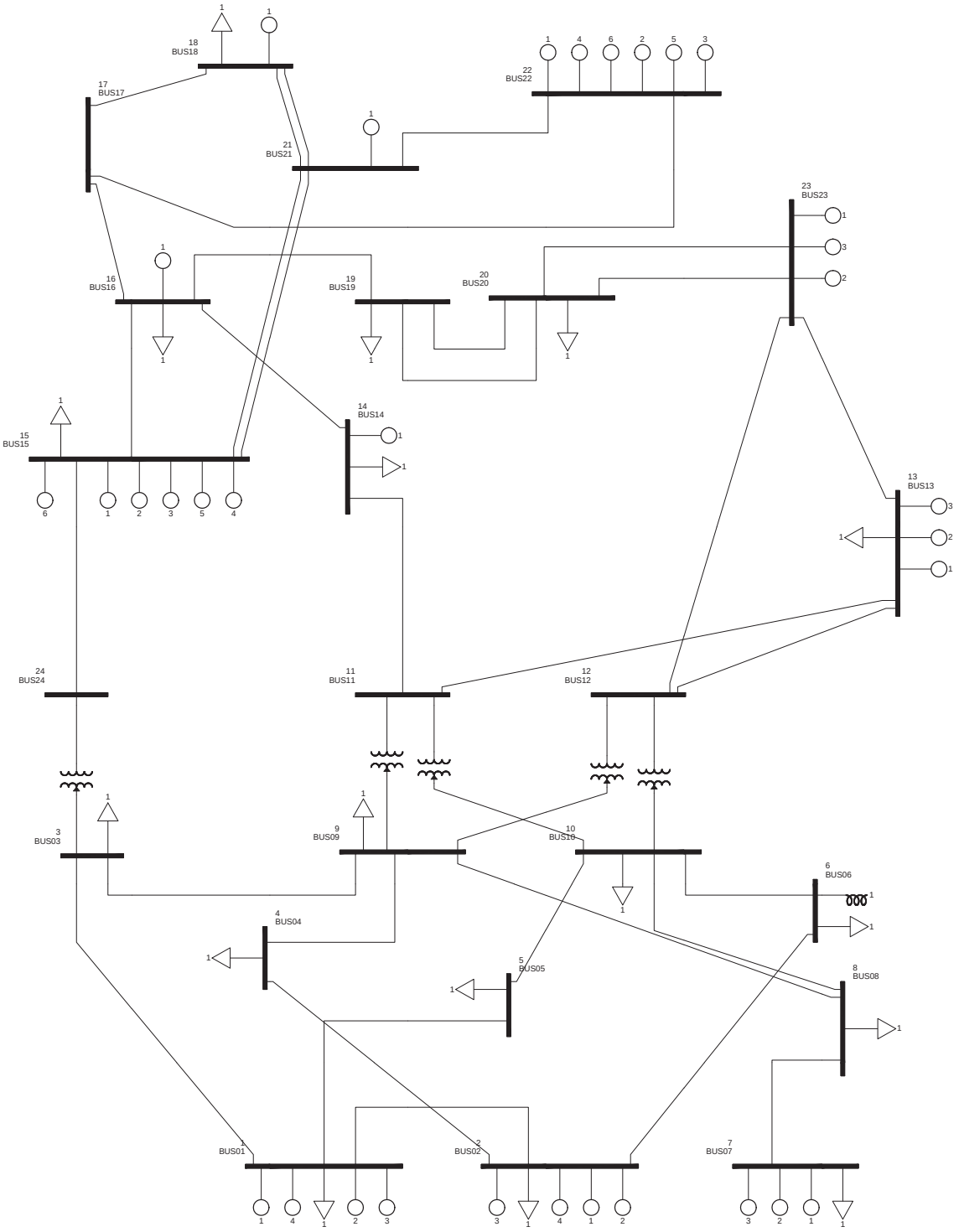

Figure 13: Power System Oneline Diagram

is 2280 MW and total generation is 2307 MW.

3.1.2 Fault Analysis Model

The fault analysis model is an addition to the power flow model, which uses the method of symmetrical components to add specific circuits which enable analysis of unbalanced faults. The power flow model contains the positive sequence model of the system, so only negative sequence and zero sequence circuit models need to be added. For this research, the negative sequence and zero sequence models were created by assuming that the negative sequence impedance is equal to the positive sequence impedance, and that the zero sequence impedance is three times the positive sequence impedance, which is within the typical range for overhead transmission lines[2][6].

3.1.3 Dynamic Analysis Model

The dynamic analysis model is an addition to the power flow model, which adds models that enable time-domain simulation of the power system. The dynamic models account for the time domain response of equipment, typically using systems of differential and algebraic equations. For this research, dynamic models were created for each of the generators using data available in the literature.

In a dynamic simulation, conventional generators are comprised of separate models which work together to represent the device. The separate models typically account for the rotor, exciter, governor, and power system stabilizers. GENROU, ESAC1A, IEESGO, and PSS2A were selected to represent these, respectively. Parameter values for each model were selected based on equipment ratings using available data provided by Anderson[3], except the power system stabilizer model parameter values were determined using an optimization feature of the software. Block diagrams and parameter values for each dynamic model used are summarized in Appendix A.

3.2 CIG Power System

3.2.1 Power Flow Model

The CIG equipment models in steady state are similar to the conventional generator models, since the particular model being used has voltage control capability. The only additional requirements for each CIG plant in the steady state model are to replace multiple unit plants with a single equivalent unit and to specify each as a wind plant with a specific control mode.

3.2.2 Fault Analysis Model

For CIG equipment, a ten percent maximum overload rating was assumed for the converter[25]. This rating limitation was imposed in the fault analysis software as a part of the generator model, in conjunction with certain solution specifications.

3.2.3 Dynamic Analysis Model

The WT4E1 and WT4G1 dynamic models were used to represent CIG in the power system. The conventional generator dynamic models were replaced by these two models to appropriately build the set of power system models. These models were developed by a large collaboration within the industry[26] to provide accurate representations of Type IV wind machines which are publicly available and do not reveal proprietary information. Block diagrams for these models are shown in Appendix A.

3.3 Complete Set of Power System Models

A set of eleven power system models was created by replacing conventional generation with CIG one plant at a time. For each progressive power system model, an entire conventional generating plant was replaced by a CIG model, representing a Type IV wind farm of equivalent capacity. This replacement was made in steady state, fault, and dynamics models. A oneline diagram of the 100% CIG power system is shown in Figure 14, including the order of plant replacement used to create the entire set

Table 6: CIG Composition of each Power System Model

	% CIG	MW CIG
Case 1	0%	0.0
Case 2	8%	174.5
Case 3	15%	349.0
Case 4	27%	621.6
Case 5	50%	1158.1
Case 6	59%	1354.1
Case 7	65%	1495.0
Case 8	81%	1858.5
Case 9	92%	2131.2
Case 10	98%	2264.1
Case 11	100%	2307.1

of cases. The plant at bus 14 is a synchronous condenser, acts as the slack bus, and was not replaced with a CIG model. The ratio of power supplied by CIG to power supplied by conventional generation for each study case is in Table 6.

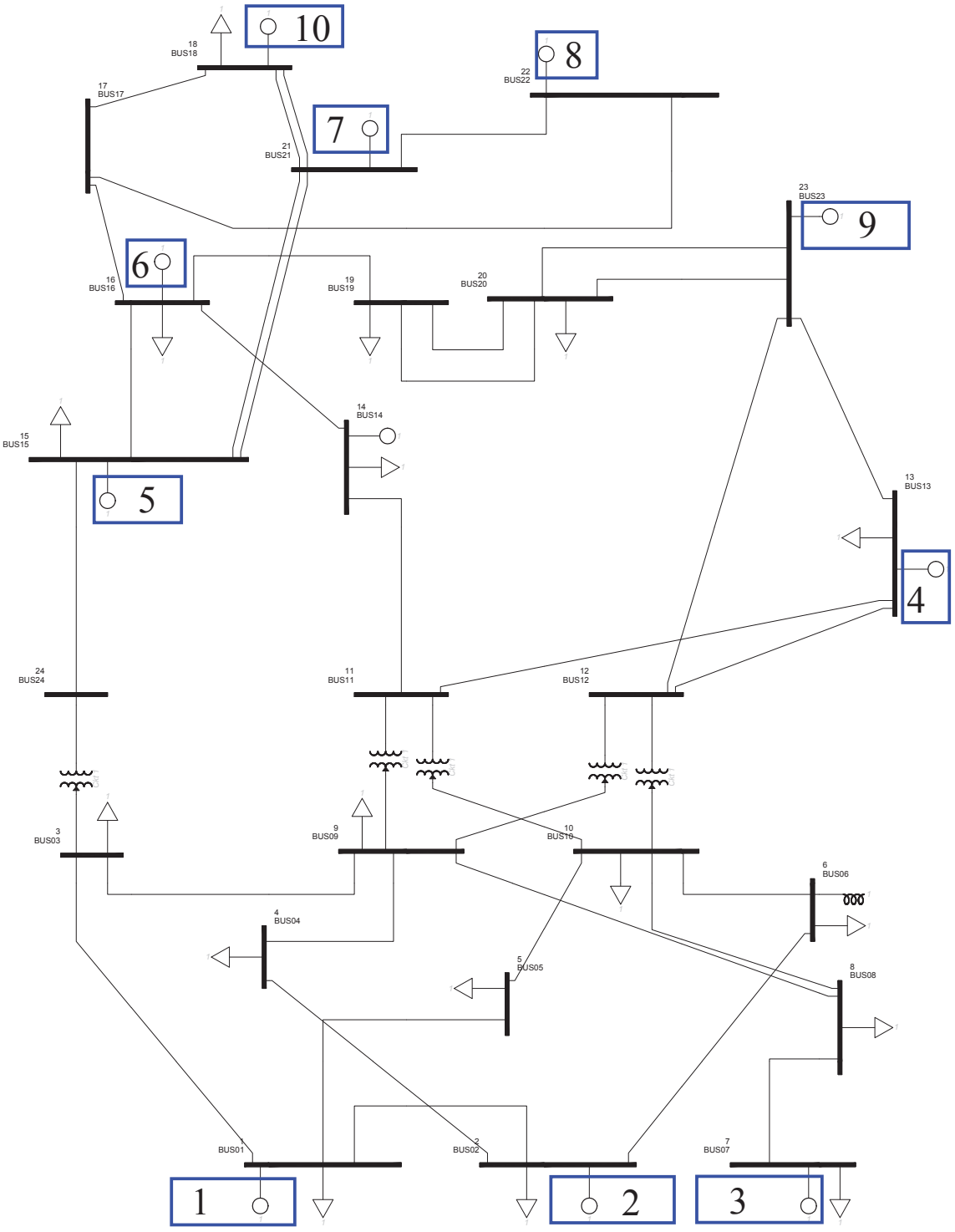

Figure 14: CIG Power System Oneline Diagram

CHAPTER 4

SIMULATION AND ANALYSIS

A comprehensive analysis has been performed on the modified RTS-24 power system at increasing levels of converter interfaced generation.

4.1 Dynamic Simulation and Analysis

Comprehensive disturbance analysis has been performed on each of the eleven dynamic cases developed. The disturbances include three-phase faults (3LG) and single-phase faults (1LG) at each transmission bus in the system, for each of the cases. A representative set of simulation results is discussed.

4.1.1 Voltage Response Through Power System Evolution

Figure 15 through Figure 25 show the voltage response of the power system to a 5-cycle 3LG fault at Bus 1, as CIG penetration increases. This fault is cleared in the simulation without tripping any circuits or other equipment in the system. Although equipment outages are required to isolate faults in a real power system, this type of disturbance simulation without outages can provide a basis for comparing system response to the fault only. It is clear that the voltage response of the system changes, exhibiting an increase in frequency of voltage oscillation with increasing CIG.

Simulations with circuit tripping to clear the fault were also simulated for 3LG, 1LG, and phase to phase (L-L) faults. Since the L-L and 1LG disturbance responses turned out to be lest severe versions of the 3LG case, only 3LG results are discussed. Figure 26 shows the bus 1 voltage response to a 3LG fault at bus 21 with the transmission line from bus 21 to bus 15 tripping to clear the fault. The simulations represent a close-in fault on the transmission line, which is cleared by local and remote circuit

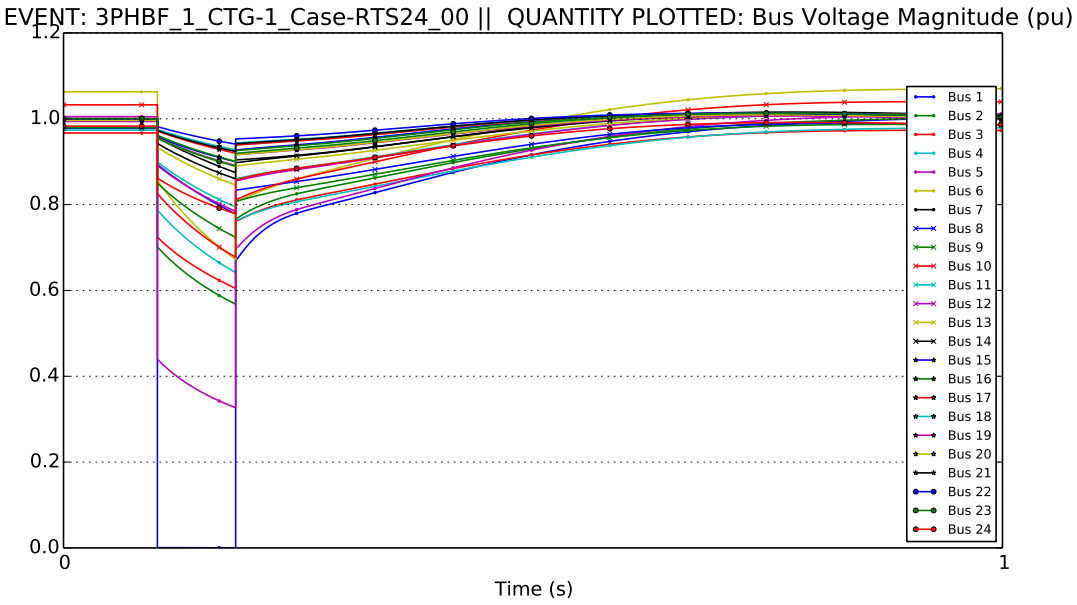

Figure 15: System bus voltage response for 0% CIG case.

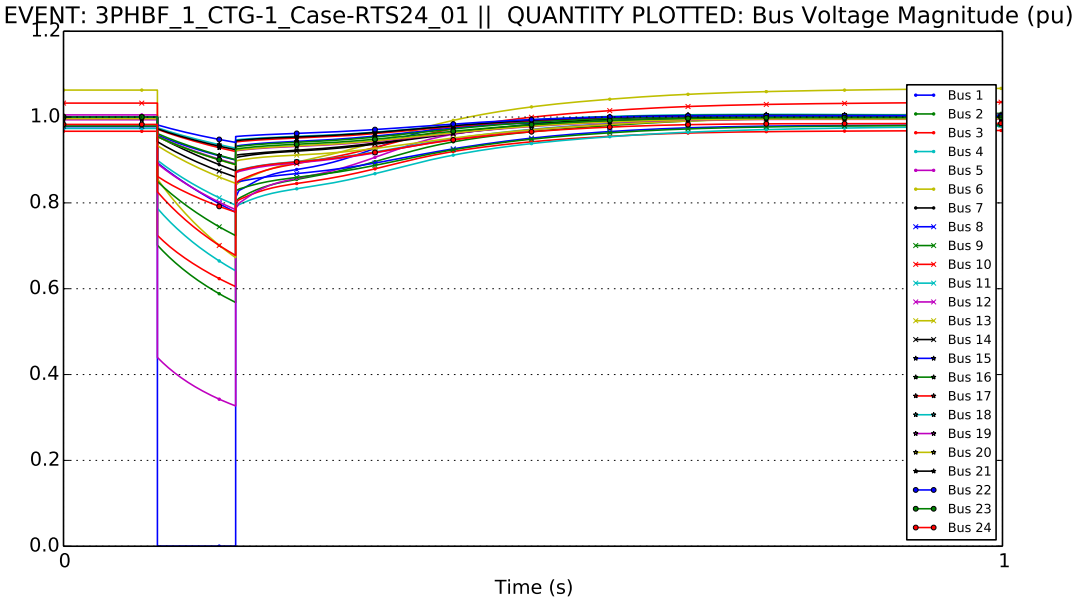

Figure 16: System bus voltage response for 8% CIG case.

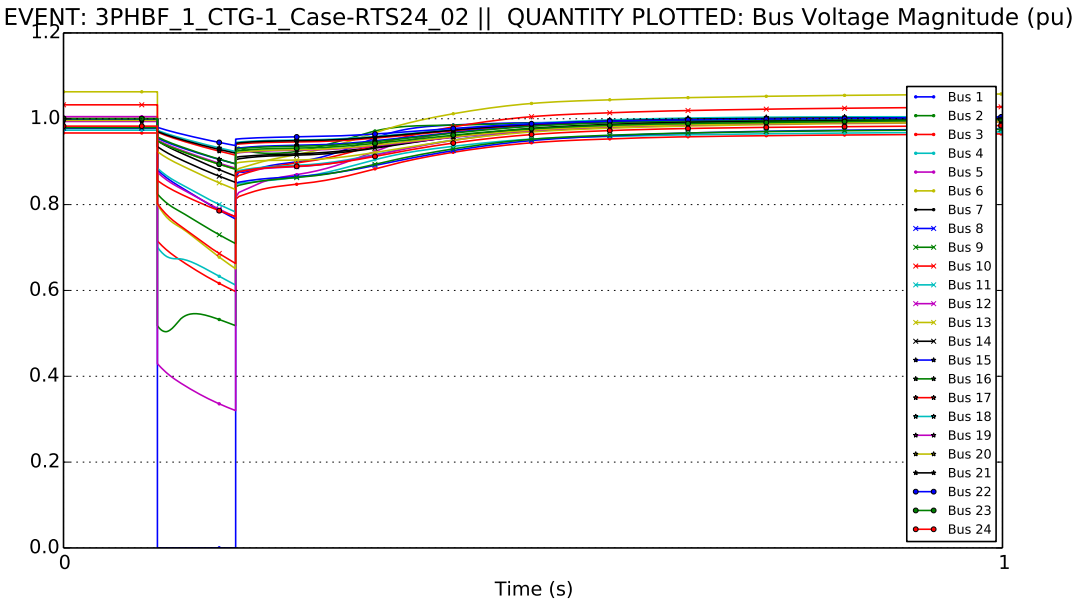

Figure 17: System bus voltage response for 15% CIG case.

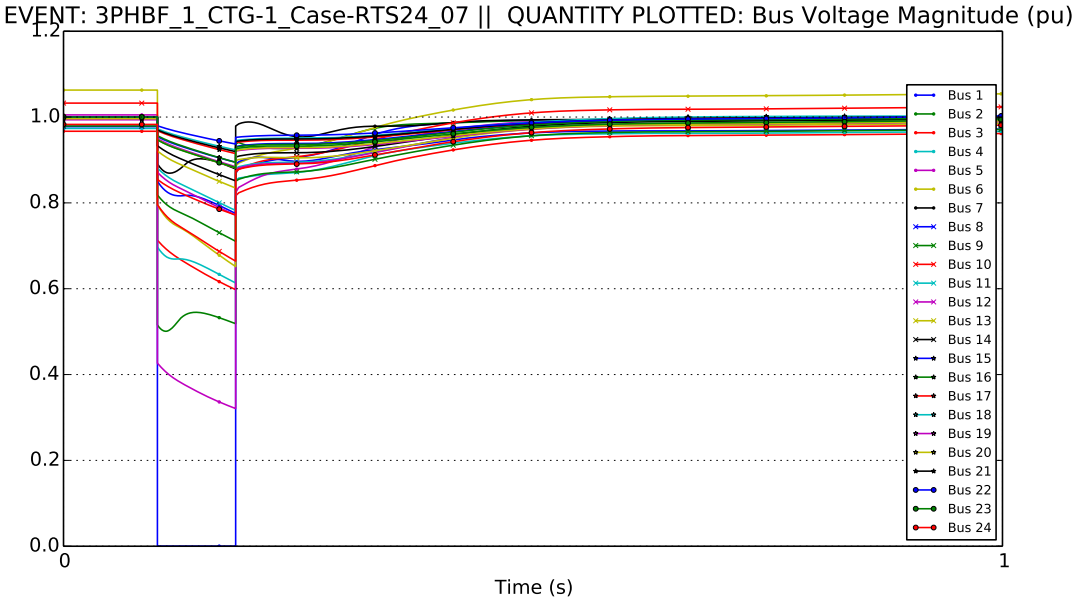

Figure 18: System bus voltage response for 27% CIG case.

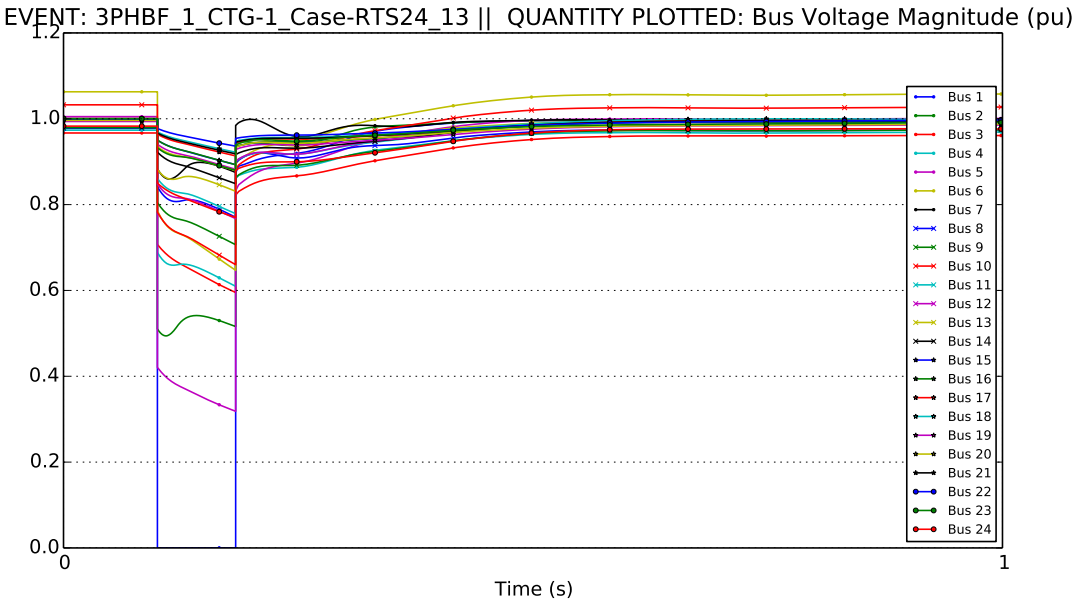

Figure 19: System bus voltage response for 50% CIG case.

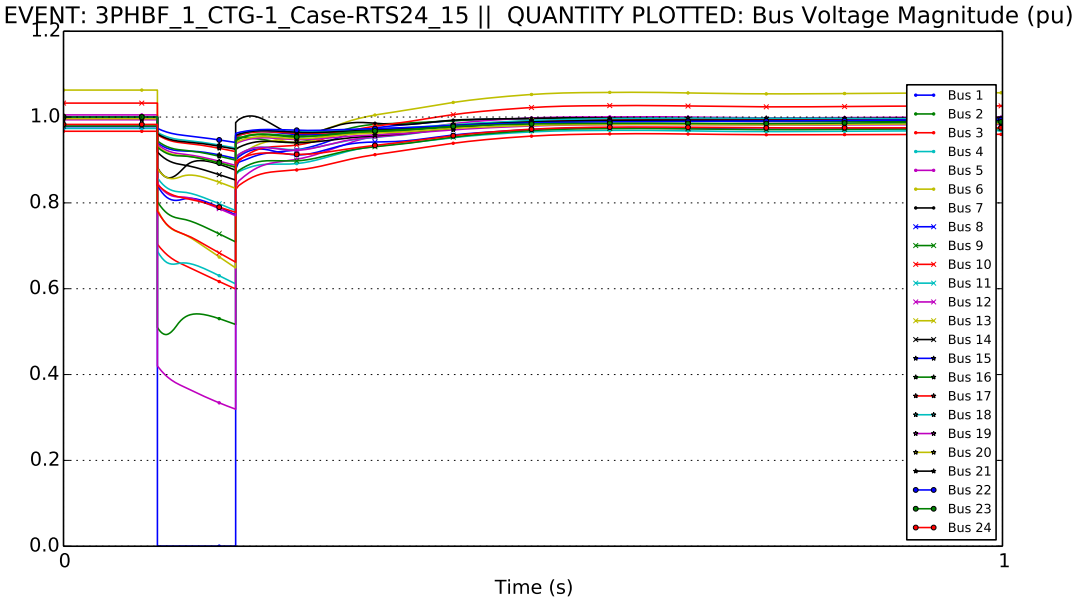

Figure 20: System bus voltage response for 59% CIG case.

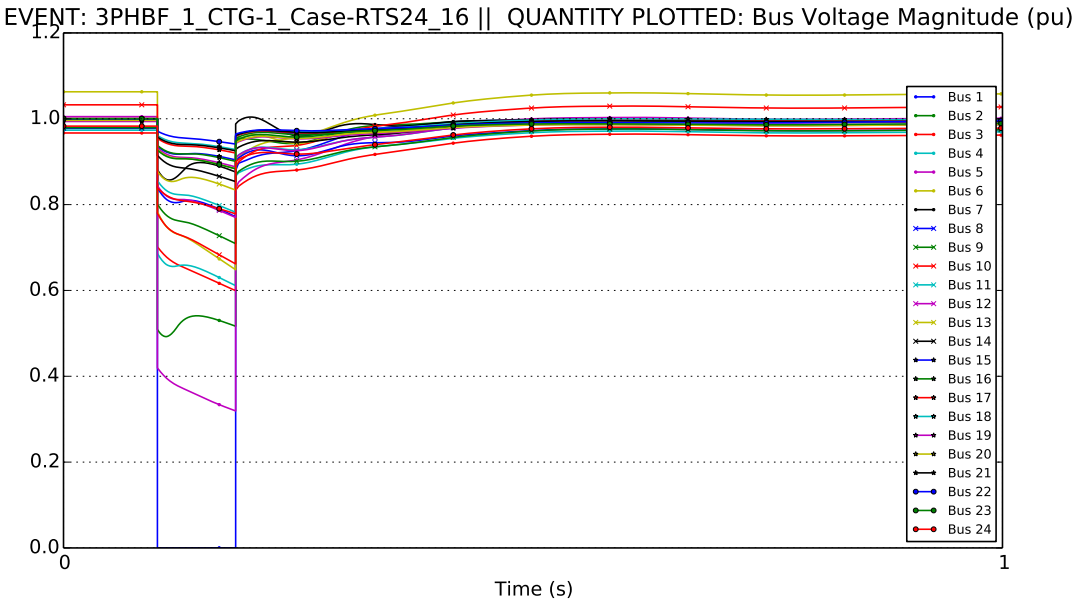

Figure 21: System bus voltage response for 65% CIG case.

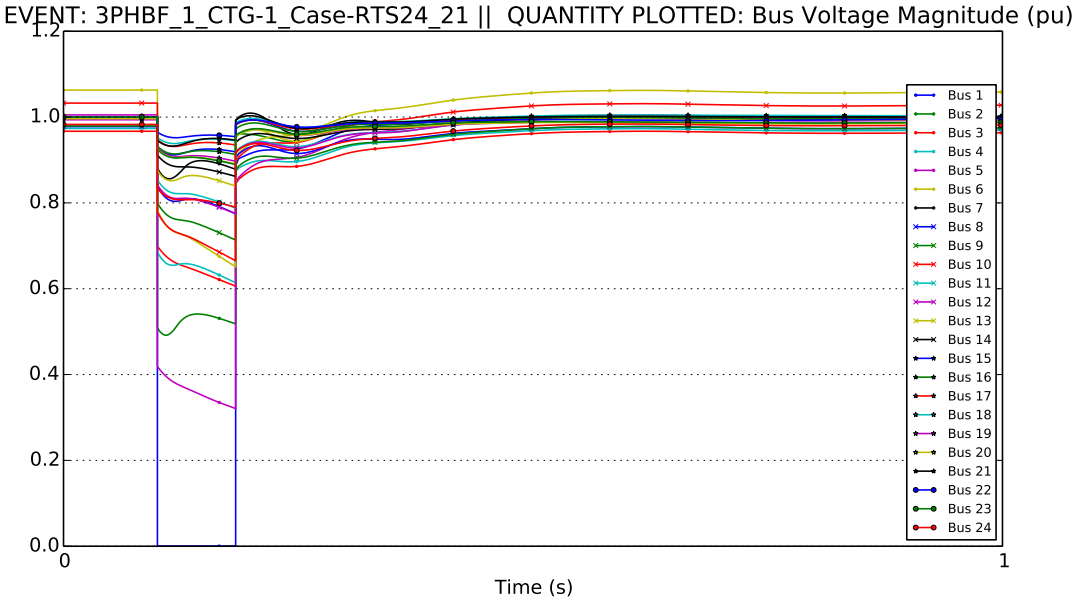

Figure 22: System bus voltage response for 81% CIG case.

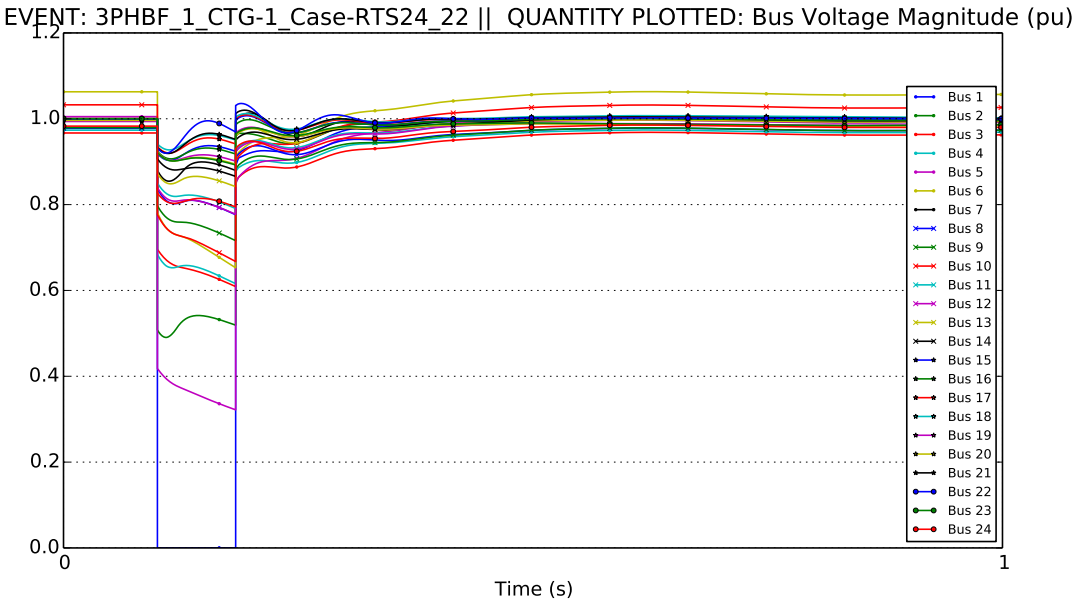

Figure 23: System bus voltage response for 92% CIG case.

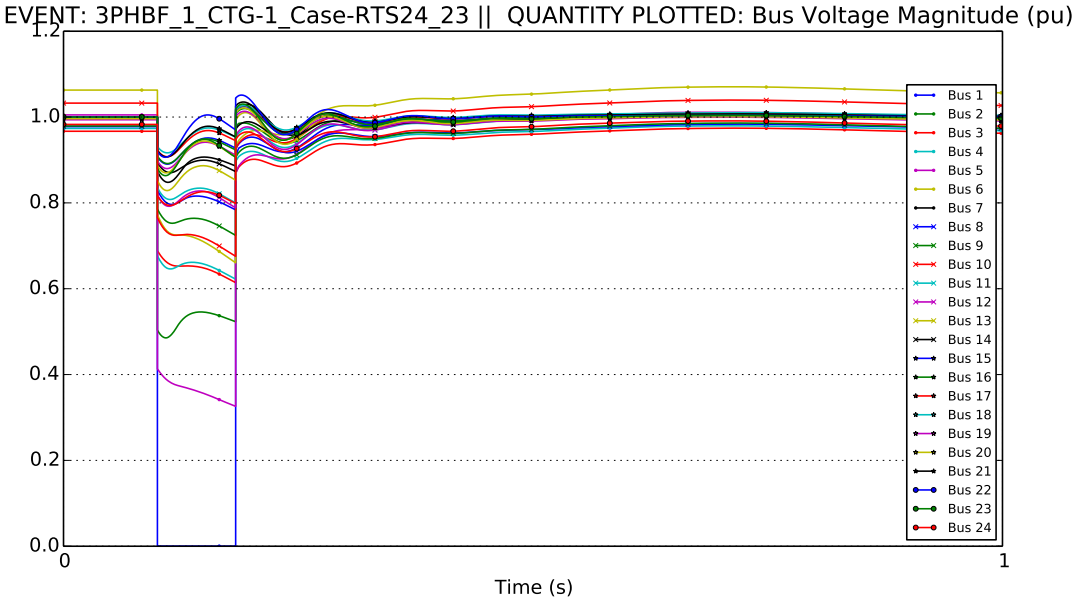

Figure 24: System bus voltage response for 98% CIG case.

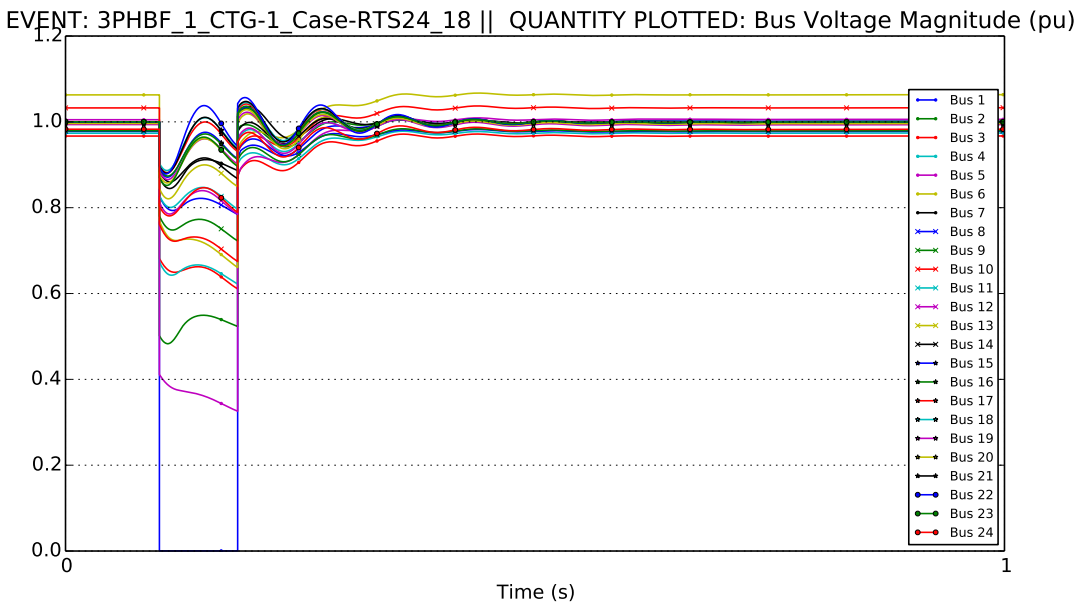

Figure 25: System bus voltage response for 100% CIG case.

breakers. The results are representative of similar disturbances at different locations in the power system.

4.1.2 Frequency Response Through Power System Evolution

Figure 27 through Figure 37 show the frequency response of the power system to a 5-cycle 3LG fault at Bus 1, as CIG penetration increase. This fault is cleared in the simulation without tripping any circuits or other equipment in the system. It is clear that the frequency response of the system changes, exhibiting more severe frequency dips with increasing CIG.

Figure 38 shows the minimum frequency experienced by a representative set of buses within the power system for the fault at Bus 1. The system frequency response gets progressively worse with increase in CIG. Large frequency dips can indicate a smaller stability margin for power systems[10].

Figure 39 shows the same minimum frequency data for the fault at Bus 1, but plotted as a function of the conventional generator power dispatch in megawatts. This plot shows the inverse linear relation between CIG penetration and conventional

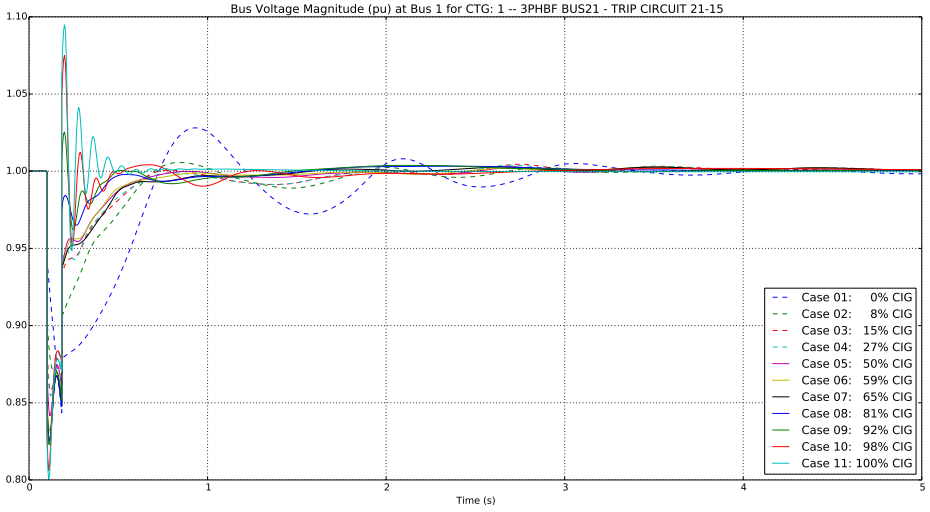

Figure 26: Bus 1 voltage response through evolution of power system for 3LG fault at bus 21 with circuit tripping.

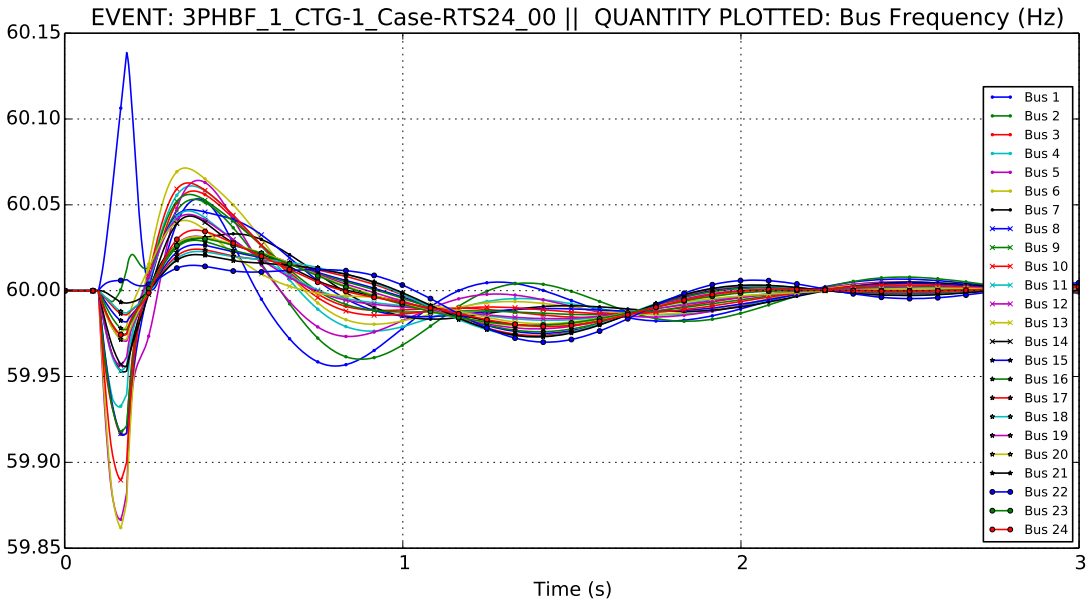

Figure 27: System bus frequency response for 0% CIG case.

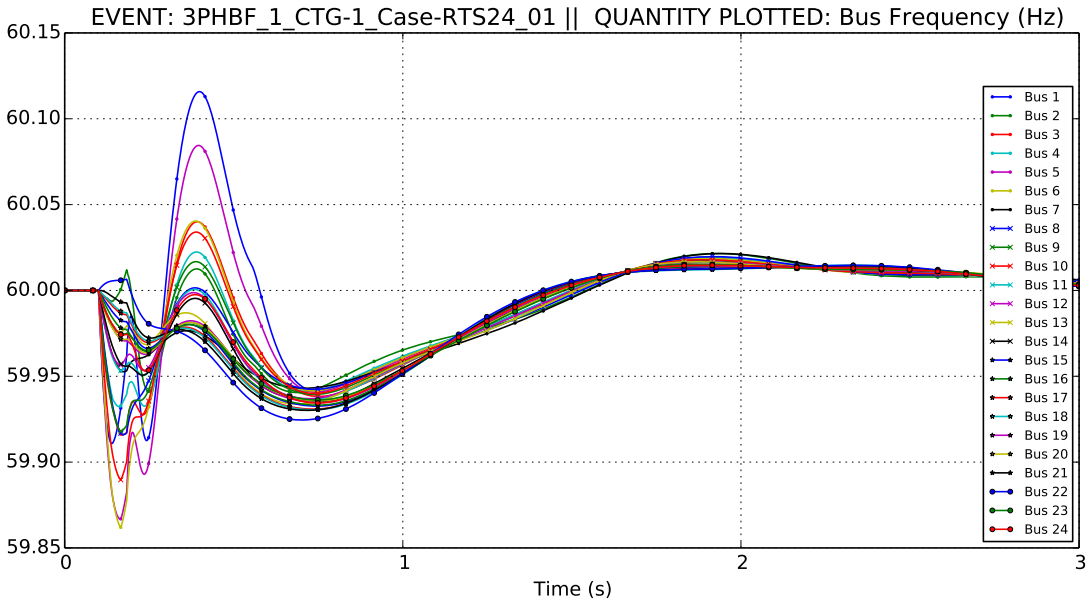

Figure 28: System bus frequency response for 8% CIG case.

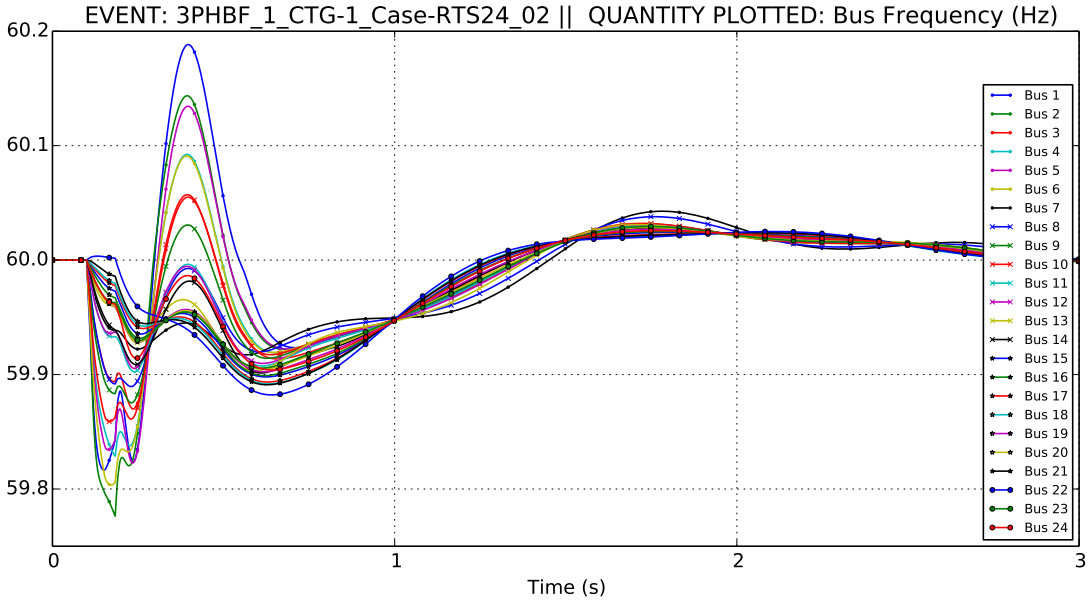

Figure 29: System bus frequency response for 15% CIG case.

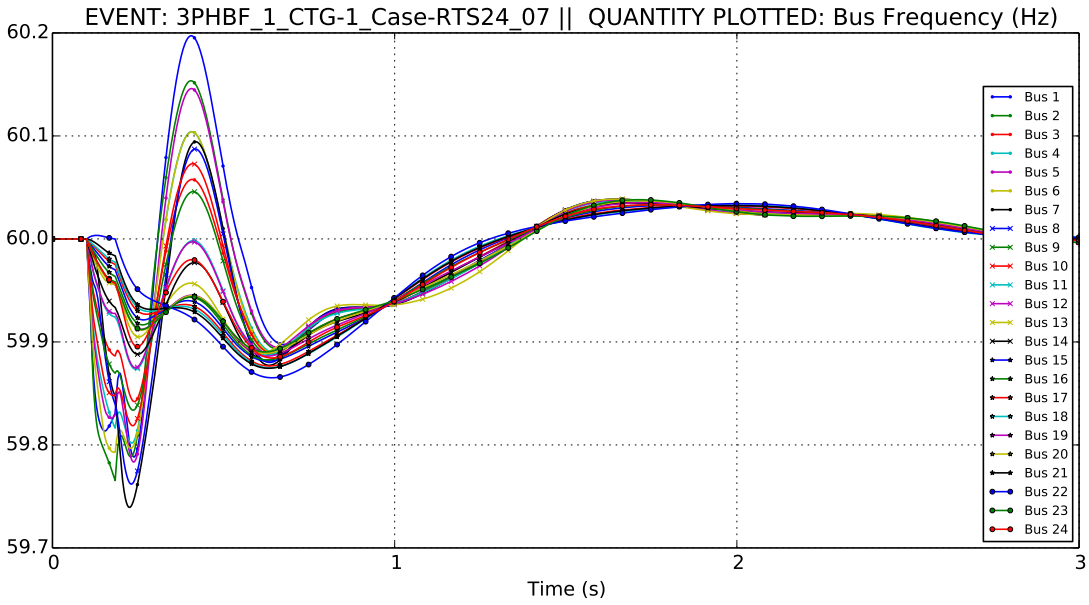

Figure 30: System bus frequency response for 27% CIG case.

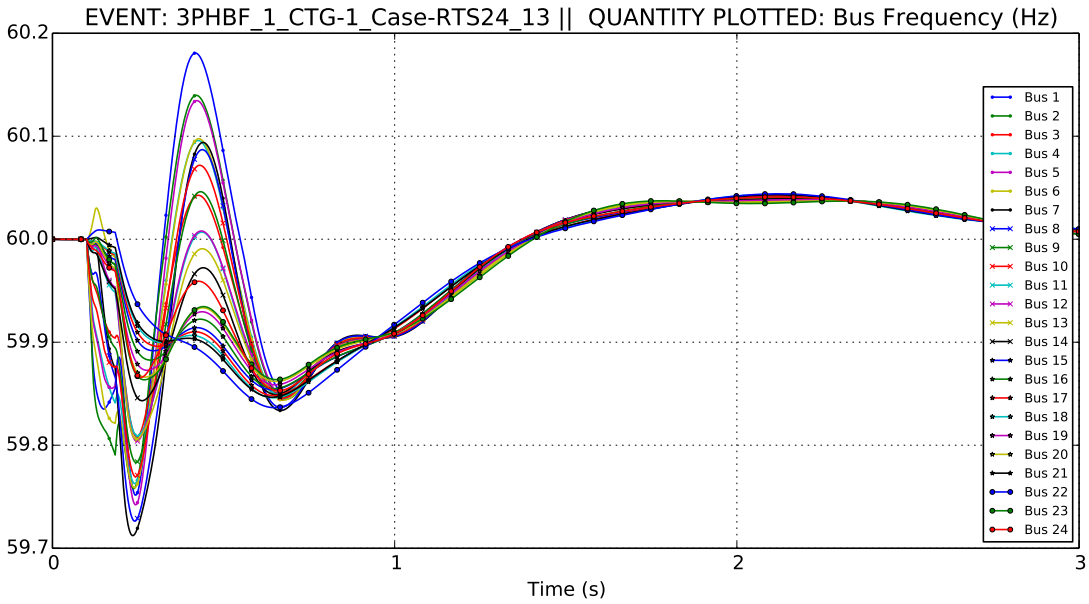

Figure 31: System bus frequency response for 50% CIG case.

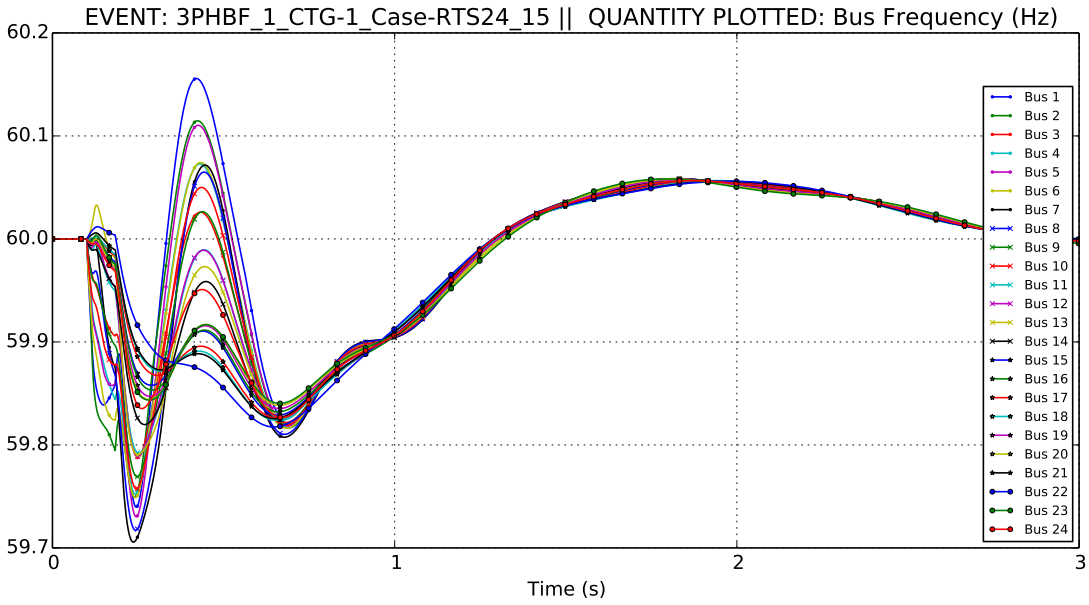

Figure 32: System bus frequency response for 59% CIG case.

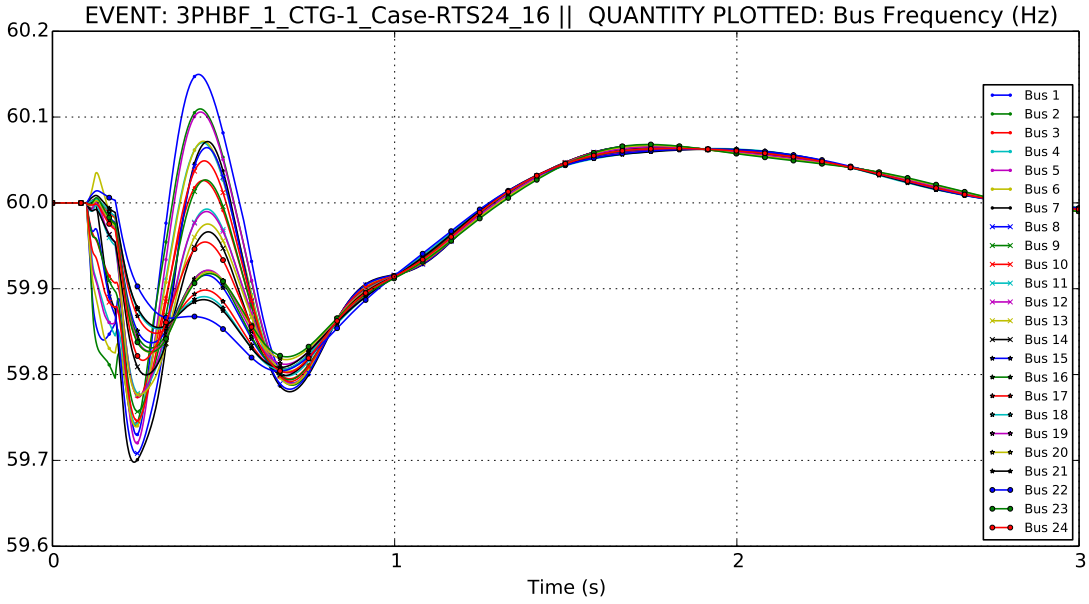

Figure 33: System bus frequency response for 65% CIG case.

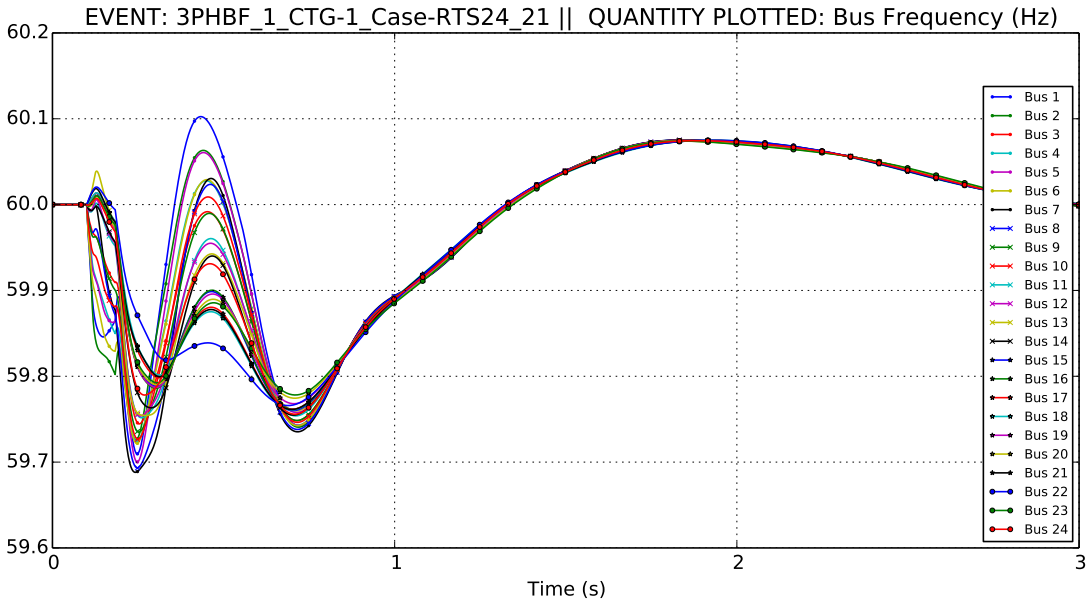

Figure 34: System bus frequency response for 81% CIG case.

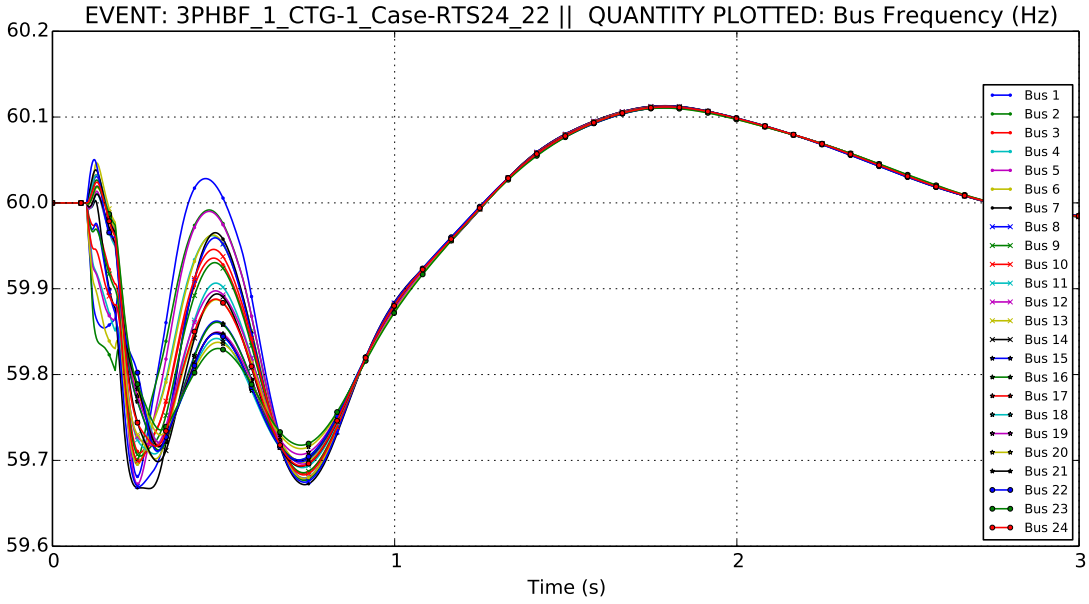

Figure 35: System bus frequency response for 92% CIG case.

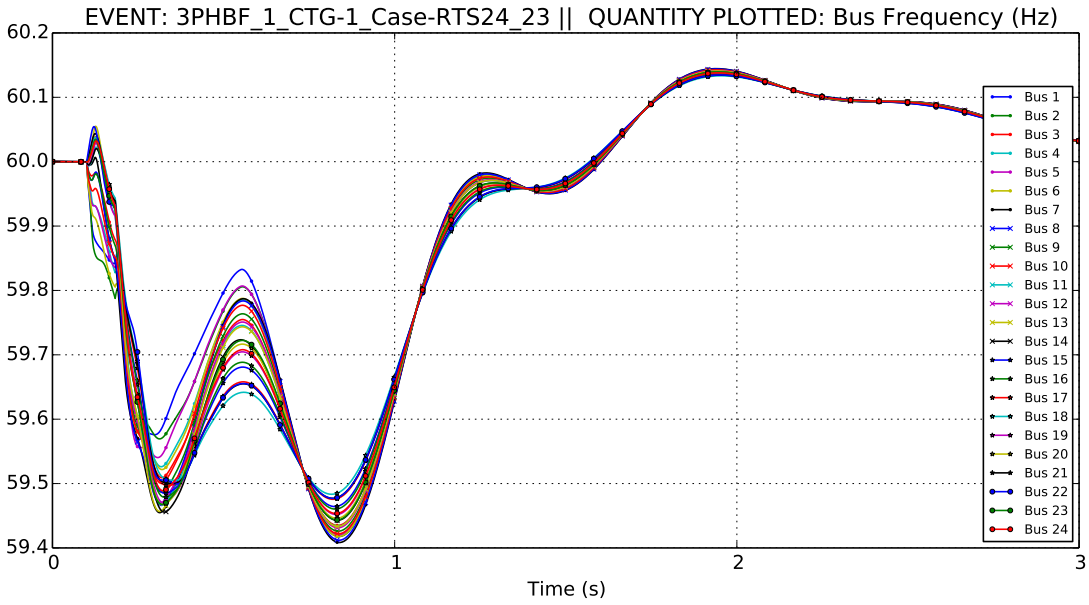

Figure 36: System bus frequency response for 98% CIG case.

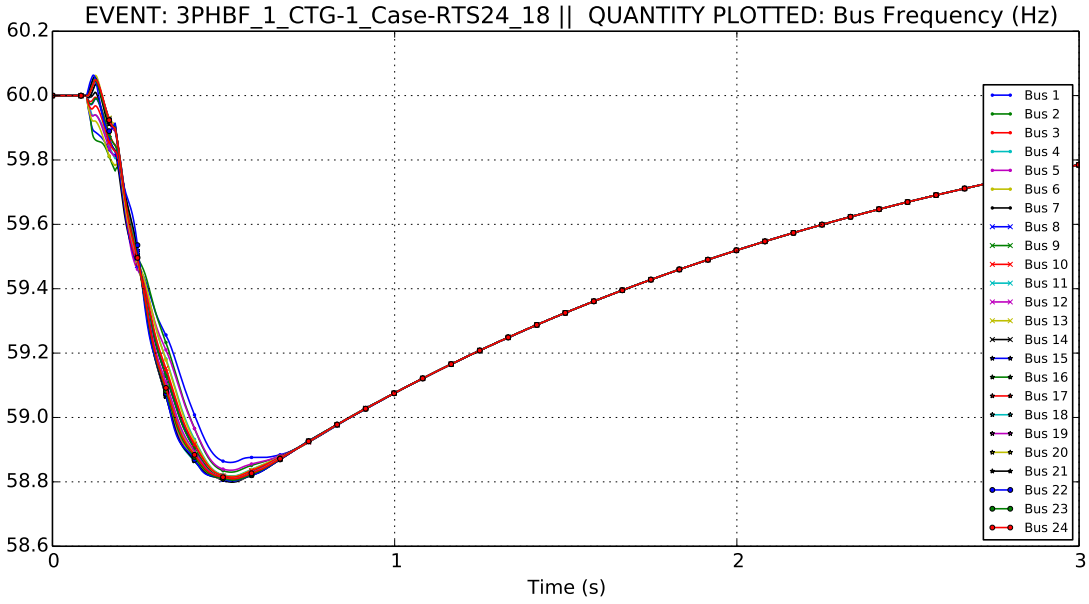

Figure 37: System bus frequency response for 100% CIG case.

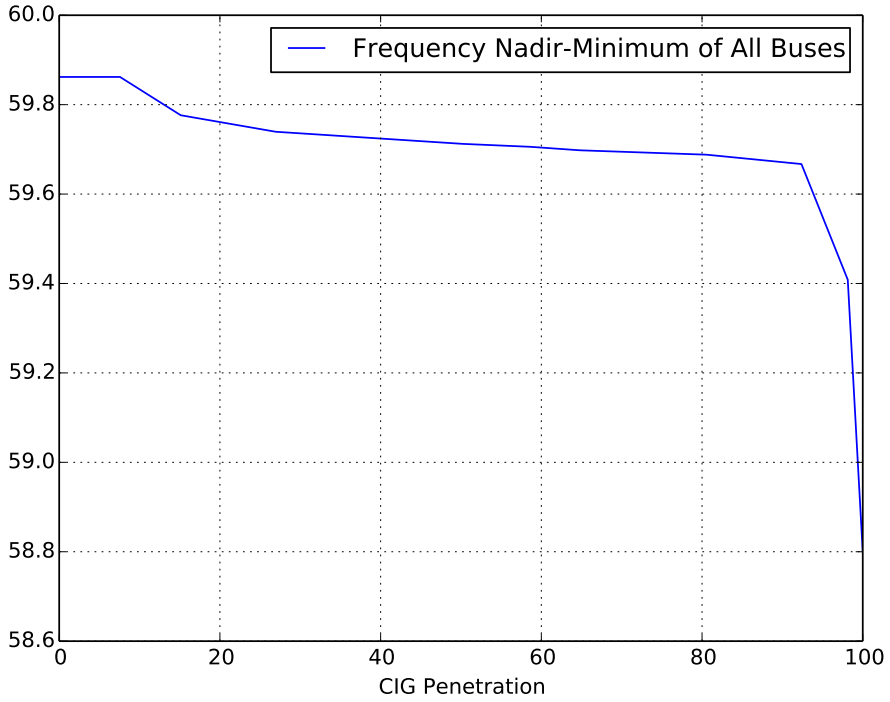

Figure 38: Minimum Bus Frequency as a function of CIG penetration

generation dispatch.

Figure 40 shows the same minimum frequency data for the fault at Bus 1, but plotted as a function of the conventional generator power capacity in megawatts. This plot shows that the relationship between CIG penetration and total conventional generation capacity is not necessarily linear, since CIG penetration is based on dispatched power and not total power capacity.

Simulations with circuit tripping to clear the fault were also simulated for 3LG, 1LG, and L-L faults. Since the L-L and 1LG disturbance responses turned out to be lest severe versions of the 3LG case, only 3LG results are discussed. Figure 41 shows the bus 1 frequency response to a 3LG fault at bus 21 with the transmission line from bus 21 to bus 15 tripping to clear the fault. These plots are representative of similar disturbances at different locations in the power system.

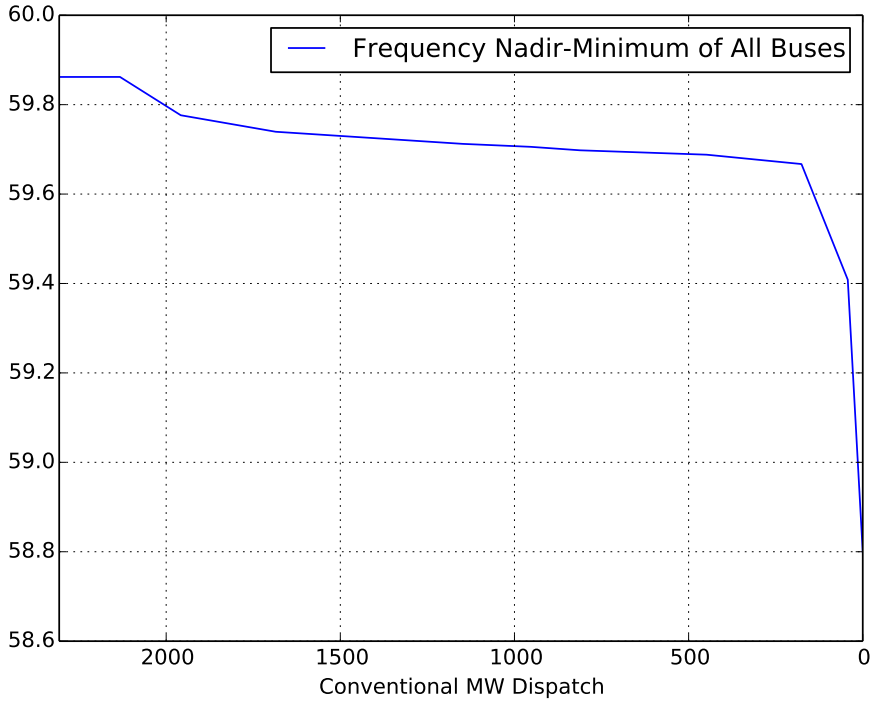

Figure 39: Minimum Bus Frequency as a function of conventional generator dispatch

4.2 Fault Simulation and Analysis

Comprehensive fault analysis has been performed on each of the eleven fault cases developed. 3LG, 1LG, and L-L fault currents were calculated at each bus in the system, for each of the cases. The fault current values appear in Table 7, Table 8, and Table 9.

The evolution of the power system results in significant changes in fault current for some buses, but meager changes for other buses. The minimal change observed in 1LG fault currents is due to numerical limitations encountered in the study method, which required a relatively high zero sequence impedance parameter value for each generator. Table 10 shows the percent decrease in fault currents from the conventional power system to the CIG power system for 3LG faults.

The reduction in fault current due to high penetration CIG systems appears to be limited by the network impedances. The power electronic converter limitations

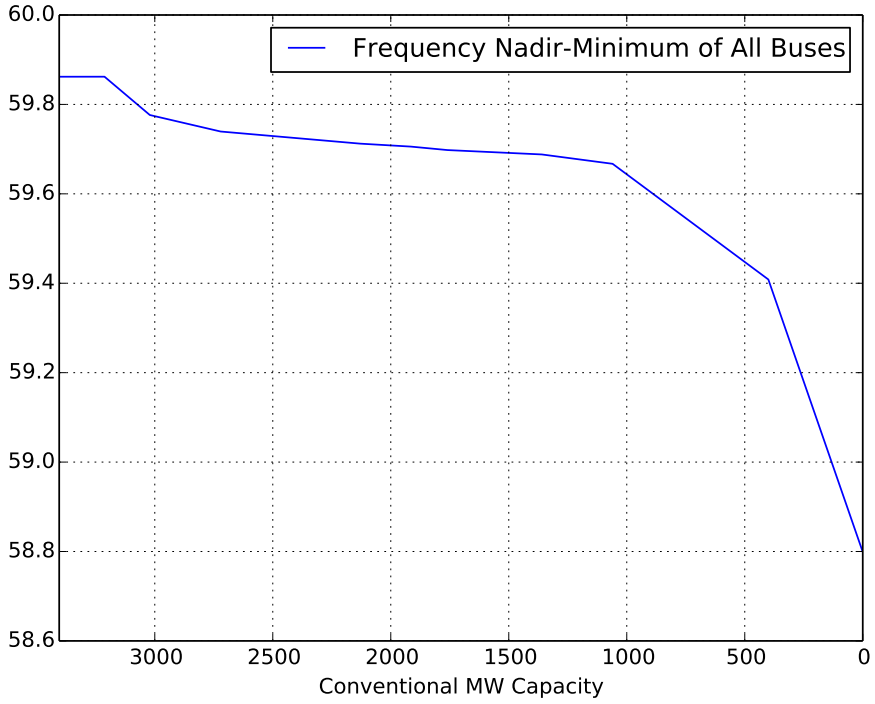

Figure 40: Minimum Bus Frequency as a function of conventional generator capacity

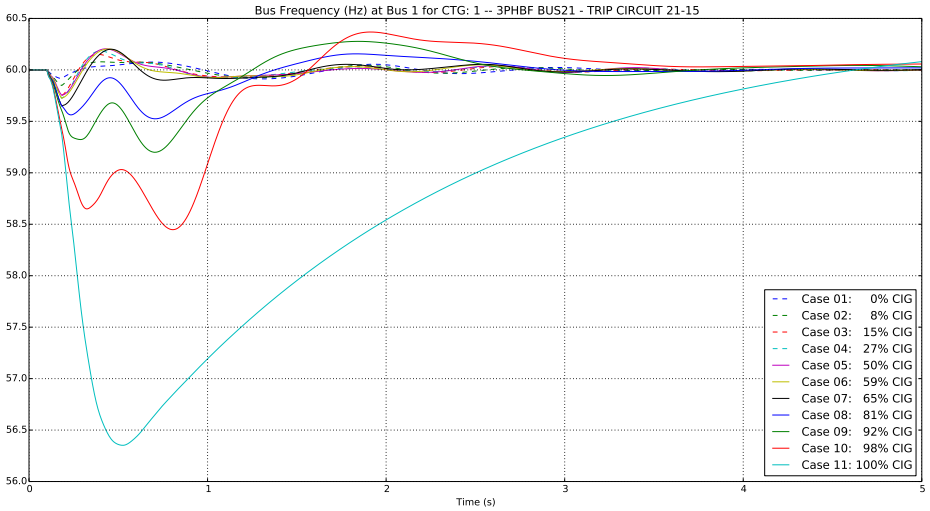

Figure 41: Bus 1 frequency response through evolution of power system for 3LG fault at bus 21 with circuit tripping.

Table 7: 3LG Fault Currents Through Evolution of Power System

Fault Bus	0%	8%	15%	27%	50%	59%	65%	81%	92%	98%	100%
BUS01	11779.7	6192.2	5631.8	5631.8	5631.8	5631.8	5631.8	5631.8	5631.8	5631.8	5631.8
BUS02	11370.1	10879.7	5294.9	5294.9	5294.9	5294.9	5294.9	5294.9	5294.9	5294.9	5294.9
BUS03	6723.9	6604.4	6588.2	6588.2	6588.2	6588.2	6588.2	6588.2	6588.2	6588.2	6588.2
BUS04	5051.6	5051.6	4631.6	4631.6	4631.6	4631.6	4631.6	4631.6	4631.6	4631.6	4631.6
BUS05	6165	5421.7	5250.4	5250.4	5250.4	5250.4	5250.4	5250.4	5250.4	5250.4	5250.4
BUS06	5592.9	5571	5317.7	5317.7	5317.7	5317.7	5317.7	5317.7	5317.7	5317.7	5317.7
BUS07	12717.5	12717.5	12717.5	3984.4	3984.4	3984.4	3984.4	3984.4	3984.4	3984.4	3984.4
BUS08	7660.1	7660.1	7660.1	5292.5	5292.5	5292.5	5292.5	5292.5	5292.5	5292.5	5292.5
BUS09	11156.1	11086.6	10764.7	10680.1	10668.5	10668.5	10668.5	10668.5	10668.5	10668.5	10668.5
BUS10	10951.8	10620.5	10152.5	10063	10044.9	10044.9	10044.9	10044.9	10044.9	10044.9	10044.9
BUS11	9716.6	9683.6	9605.5	9605.5	8600.4	8600.4	8590.2	8590.2	8590.2	8590.2	8590.2
BUS12	8940.6	8911.6	8840.3	8840.3	7838.5	7838.5	7838.5	7838.5	7838.5	7666	7666
BUS13	19023	19004.4	18957.7	18957.7	8603.3	8603.3	8603.3	8603.3	8603.3	8194.7	8194.7
BUS14	9380.7	9380.7	9380.7	9380.7	9370.8	9362.4	9220.4	9220.4	9220.4	9220.4	9220.4
BUS15	22126.1	22124.7	22124.7	22124.7	22124.7	14789.9	14015.4	12727.7	12412.4	12412.4	10499.3
BUS16	20730.8	20730.8	20730.8	20730.8	20730.8	18533	15808.6	14947	14608.7	13899.5	11643
BUS17	15404.3	15404.3	15404.3	15404.3	15404.3	14950.4	14454.6	13439.9	12612.6	12612.6	9240.7
BUS18	21281.8	21281.8	21281.8	21281.8	21281.8	20577.4	20182.1	17172.7	16034.2	16034.2	9047.4
BUS19	12035.4	12035.4	12035.4	12035.4	12035.4	11882.5	11477.9	11477.9	11477.9	9860.9	9823.3
BUS20	14176.7	14176.7	14176.7	14176.7	14132.3	14124.1	13979.1	13979.1	13979.1	8849.4	8849.4
BUS21	23363.6	23363.6	23363.6	23363.6	23363.6	21751	21321.1	14334.3	13024.5	13024.5	9253.6
BUS22	11129.7	11129.7	11129.7	11129.7	11129.7	11129.7	11129.7	11040.8	5760.3	5760.3	5654.3
BUS23	21119.6	21119.6	21119.6	21119.6	20486.3	20486.3	20375.9	20375.9	20375.9	8806.8	8806.8
BUS24	5118.5	5118.5	5118.5	5118.5	5118.5	5018.1	5018.1	5018.1	5018.1	5018.1	5018.1

Table 8: L-L Fault Currents Through Evolution of Power System

Fault Bus	0%	8%	15%	27%	50%	59%	65%	81%	92%	98%	100%
BUS01	10201.5	5215.9	4564	4564	4564	4564	4564	4564	4564	4564	4564
BUS02	9846.8	9374.3	4270.5	4270.5	4270.5	4270.5	4270.5	4270.5	4270.5	4270.5	4270.5
BUS03	5823.1	5683.7	5606.6	5606.6	5606.6	5606.6	5606.6	5606.6	5606.6	5606.6	5606.6
BUS04	4374.8	4356.2	3888.9	3888.9	3888.9	3888.9	3888.9	3888.9	3888.9	3888.9	3888.9
BUS05	5339	4646.9	4407.1	4407.1	4407.1	4407.1	4407.1	4407.1	4407.1	4407.1	4407.1
BUS06	4843.6	4794.9	4490.5	4490.5	4490.5	4490.5	4490.5	4490.5	4490.5	4490.5	4490.5
BUS07	11013.7	11013.7	11013.7	3225.8	3225.8	3225.8	3225.8	3225.8	3225.8	3225.8	3225.8
BUS08	6633.9	6626.9	6607.9	4435.6	4435.6	4435.6	4435.6	4435.6	4435.6	4435.6	4435.6
BUS09	9661.4	9562.5	9190.4	9000.2	8812.7	8812.7	8812.7	8812.7	8812.7	8812.7	8812.7
BUS10	9484.5	9153.8	8648.9	8455.4	8267.1	8267.1	8267.1	8267.1	8267.1	8267.1	8267.1
BUS11	8414.8	8361.6	8239.2	8214	7246.6	7246.6	7226.2	7226.2	7226.2	7226.2	7226.2
BUS12	7742.8	7694.1	7579.6	7558.2	6598.7	6598.7	6598.7	6598.7	6598.7	6357.1	6357.1
BUS13	16474.4	16438.5	16351.7	16347.4	7222.3	7222.3	7215.1	7215.1	7215.1	6736.1	6736.1
BUS14	8123.9	8119.2	8109.7	8109.7	8034.1	7999.5	7860.3	7860.3	7860.3	7860.3	7860.3
BUS15	19161.7	19146.2	19137	19137	19137	12792.3	12090.1	10941.6	10673.5	10650.5	8813.3
BUS16	17953.4	17945	17936.3	17936.3	17901.3	15991.2	13607.8	12830.2	12540	11708.6	9597.8
BUS17	13340.5	13340.5	13340.5	13340.5	13340.5	12944	12513.1	11640.9	10950	10950	7903.4
BUS18	18430.5	18430.5	18430.5	18430.5	18430.5	17825.1	17480.1	14894.8	13934.1	13934.1	7686.1
BUS19	10422.9	10422.9	10422.9	10422.9	10422.9	10275.7	9923	9917.1	9917.1	8362.1	8221.3
BUS20	12277.4	12277.4	12277.4	12277.4	12195.4	12165.7	12026.5	12026.5	12026.5	7458.2	7458.2
BUS21	20233.4	20233.4	20233.4	20233.4	20233.4	18857.6	18478.9	12407.2	11283.5	11283.5	7854.9
BUS22	9638.6	9638.6	9638.6	9638.6	9638.6	9638.6	9637.6	9556.2	5044.3	5044.3	4872.8
BUS23	18290.1	18286.6	18279.3	18279.3	17650.9	17623.1	17502	17502	17502	7329.1	7329.1
BUS24	4432.8	4419	4418	4418	4418	4310.9	4304.9	4304.9	4304.9	4304.9	4304.9

Table 9: 1LG Fault Currents Through Evolution of Power System

Fault Bus	0%	8%	15%	27%	50%	59%	65%	81%	92%	98%	100%
BUS01	10201.5	5215.9	4564	4564	4564	4564	4564	4564	4564	4564	4564
BUS02	9846.8	9374.3	4270.5	4270.5	4270.5	4270.5	4270.5	4270.5	4270.5	4270.5	4270.5
BUS03	5823.1	5683.7	5606.6	5606.6	5606.6	5606.6	5606.6	5606.6	5606.6	5606.6	5606.6
BUS04	4374.8	4356.2	3888.9	3888.9	3888.9	3888.9	3888.9	3888.9	3888.9	3888.9	3888.9
BUS05	5339	4646.9	4407.1	4407.1	4407.1	4407.1	4407.1	4407.1	4407.1	4407.1	4407.1
BUS06	4843.6	4794.9	4490.5	4490.5	4490.5	4490.5	4490.5	4490.5	4490.5	4490.5	4490.5
BUS07	11013.7	11013.7	11013.7	3225.8	3225.8	3225.8	3225.8	3225.8	3225.8	3225.8	3225.8
BUS08	6633.9	6626.9	6607.9	4435.6	4435.6	4435.6	4435.6	4435.6	4435.6	4435.6	4435.6
BUS09	9661.4	9562.5	9190.4	9000.2	8812.7	8812.7	8812.7	8812.7	8812.7	8812.7	8812.7
BUS10	9484.5	9153.8	8648.9	8455.4	8267.1	8267.1	8267.1	8267.1	8267.1	8267.1	8267.1
BUS11	8414.8	8361.6	8239.2	8214	7246.6	7246.6	7226.2	7226.2	7226.2	7226.2	7226.2
BUS12	7742.8	7694.1	7579.6	7558.2	6598.7	6598.7	6598.7	6598.7	6598.7	6357.1	6357.1
BUS13	16474.4	16438.5	16351.7	16347.4	7222.3	7222.3	7215.1	7215.1	7215.1	6736.1	6736.1
BUS14	8123.9	8119.2	8109.7	8109.7	8034.1	7999.5	7860.3	7860.3	7860.3	7860.3	7860.3
BUS15	19161.7	19146.2	19137	19137	19137	12792.3	12090.1	10941.6	10673.5	10650.5	8813.3
BUS16	17953.4	17945	17936.3	17936.3	17901.3	15991.2	13607.8	12830.2	12540	11708.6	9597.8
BUS17	13340.5	13340.5	13340.5	13340.5	13340.5	12944	12513.1	11640.9	10950	10950	7903.4
BUS18	18430.5	18430.5	18430.5	18430.5	18430.5	17825.1	17480.1	14894.8	13934.1	13934.1	7686.1
BUS19	10422.9	10422.9	10422.9	10422.9	10422.9	10275.7	9923	9917.1	9917.1	8362.1	8221.3
BUS20	12277.4	12277.4	12277.4	12277.4	12195.4	12165.7	12026.5	12026.5	12026.5	7458.2	7458.2
BUS21	20233.4	20233.4	20233.4	20233.4	20233.4	18857.6	18478.9	12407.2	11283.5	11283.5	7854.9
BUS22	9638.6	9638.6	9638.6	9638.6	9638.6	9638.6	9637.6	9556.2	5044.3	5044.3	4872.8
BUS23	18290.1	18286.6	18279.3	18279.3	17650.9	17623.1	17502	17502	17502	7329.1	7329.1
BUS24	4432.8	4419	4418	4418	4418	4310.9	4304.9	4304.9	4304.9	4304.9	4304.9

Table 10: Fault Current Percent Decrease From Conventional to CIG Power System

BUS	3LG
BUS01	52.19 %
BUS02	53.43 %
BUS03	2.02 %
BUS04	8.31 %
BUS05	14.84 %
BUS06	4.92 %
BUS07	68.67 %
BUS08	30.91 %
BUS09	4.37 %
BUS10	8.28 %
BUS11	11.59 %
BUS12	14.26 %
BUS13	56.92 %
BUS14	1.71 %
BUS15	52.55 %
BUS16	43.84 %
BUS17	40.01 %
BUS18	57.49 %
BUS19	18.38 %
BUS20	37.58 %
BUS21	60.39 %
BUS22	49.20 %
BUS23	58.30 %
BUS24	1.96 %

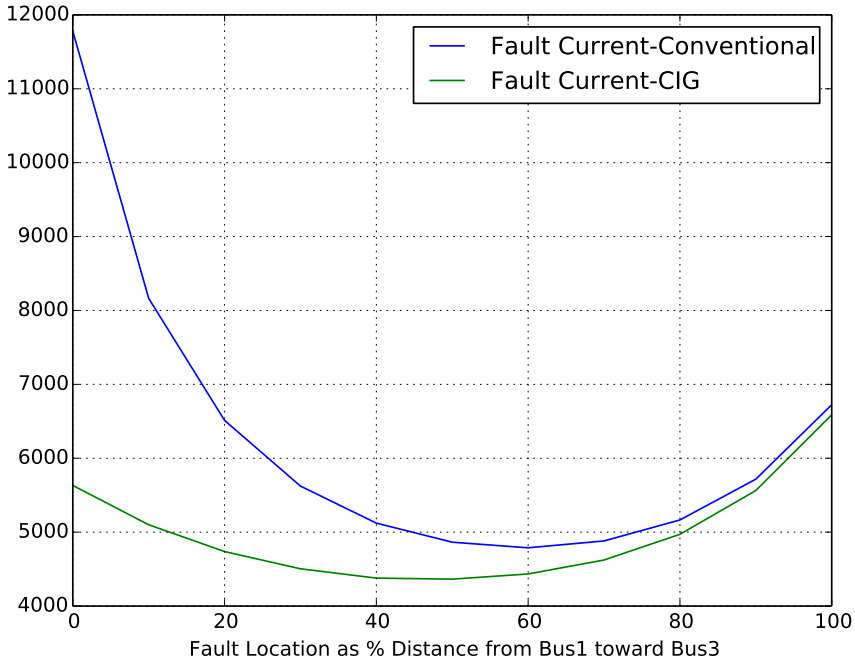

Figure 42: Fault currents from Bus 1 toward Bus 3

appear most significant for faults near the converter, and become less prominent as the fault moves away from the converter. Figure 42 shows the fault current for faults beginning at Bus 1 and moving toward Bus 3 in 10% increments. Results for the conventional power system and the 100% CIG power system are shown. Bus 1 has a generating plant connected to it, while Bus 3 has the low-side of a transformer connected to it. As the fault progresses from a source into the network, the difference in fault currents for the two systems becomes insignificant.

Figure 43 shows the fault current for faults beginning at Bus 23 and moving toward Bus 12 in 10% increments. Results for the conventional power system and the 100% CIG power system are shown. Bus 23 has a generating plant connected to it, while Bus 12 has the high-side of a transformer connected to it. As the fault progresses from a source into the network, the difference in fault currents for the two systems becomes insignificant.

Figure 44 shows the fault current for faults beginning at Bus 19 and moving toward

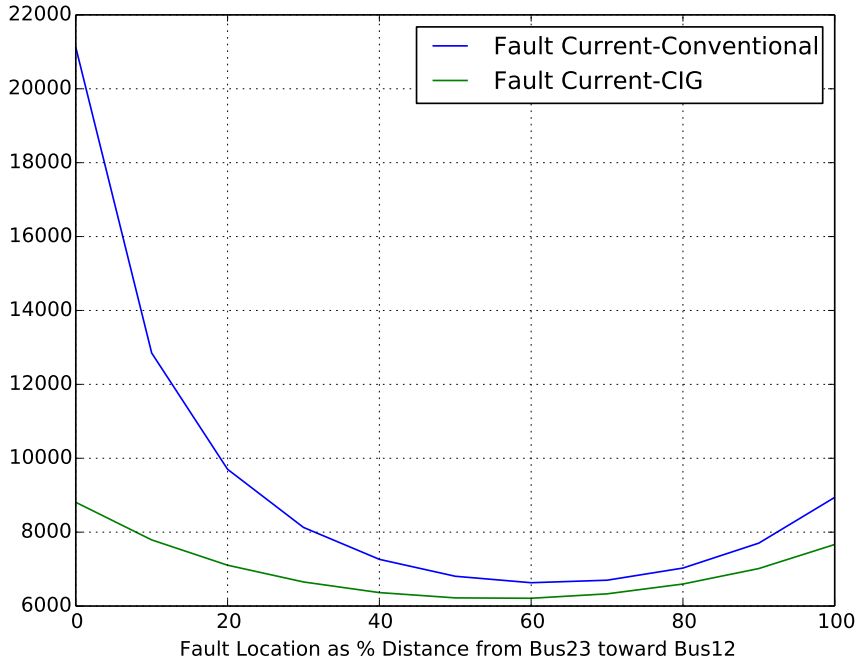

Figure 43: Fault currents from Bus 23 toward Bus 12

Bus 20 in 10% increments. Results for the conventional power system and the 100% CIG power system are shown. Bus 19 and Bus 20 are in the middle of the power system, relatively remote from sources. As the fault progresses from one bus remote from source to another bus remote from sources, the difference in fault currents for the two systems is relatively unchanged.

Figure 45 shows the fault current for faults beginning at Bus 7 and moving toward Bus 8 in 10% increments. Results for the conventional power system and the 100% CIG power system are shown. Bus 7 has a generating plant connected to it which is radially connected to Bus 8 through a single transmission line. As the fault progresses from a source into the network along the radial transmission line, the difference in fault currents for the two systems becomes less.

Figure 46 shows the fault current for faults beginning at Bus 13 and moving toward Bus 23 in 10% increments. Results for the conventional power system and the 100% CIG power system are shown. Bus 13 and Bus 23 have generating plants connected.

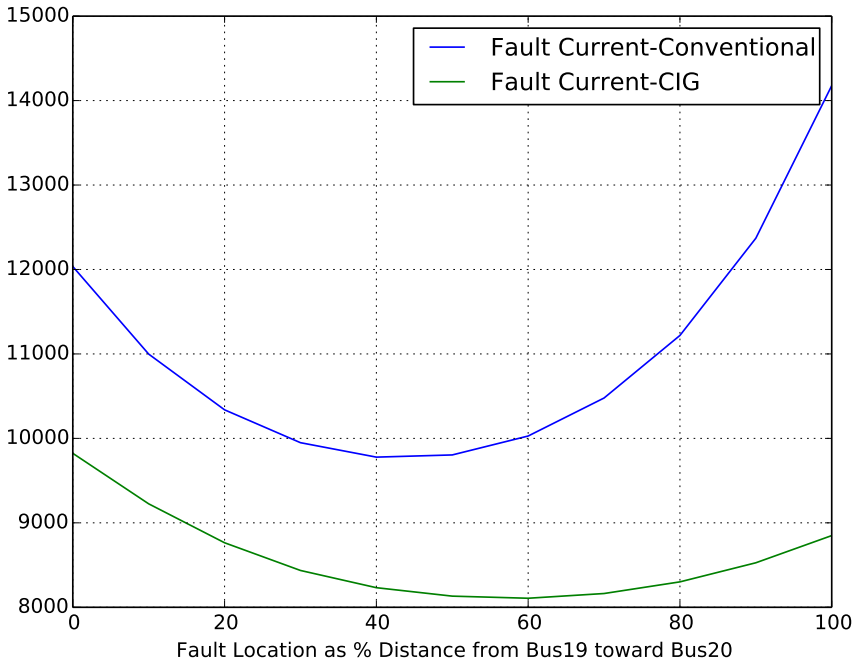

Figure 44: Fault currents from Bus 19 toward Bus 20

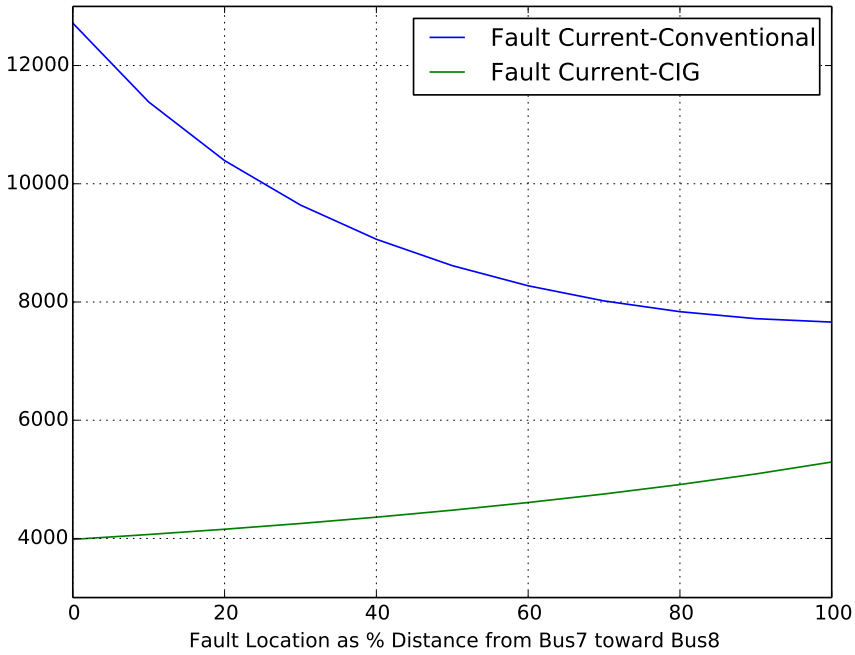

Figure 45: Fault currents from Bus 7 toward Bus 8

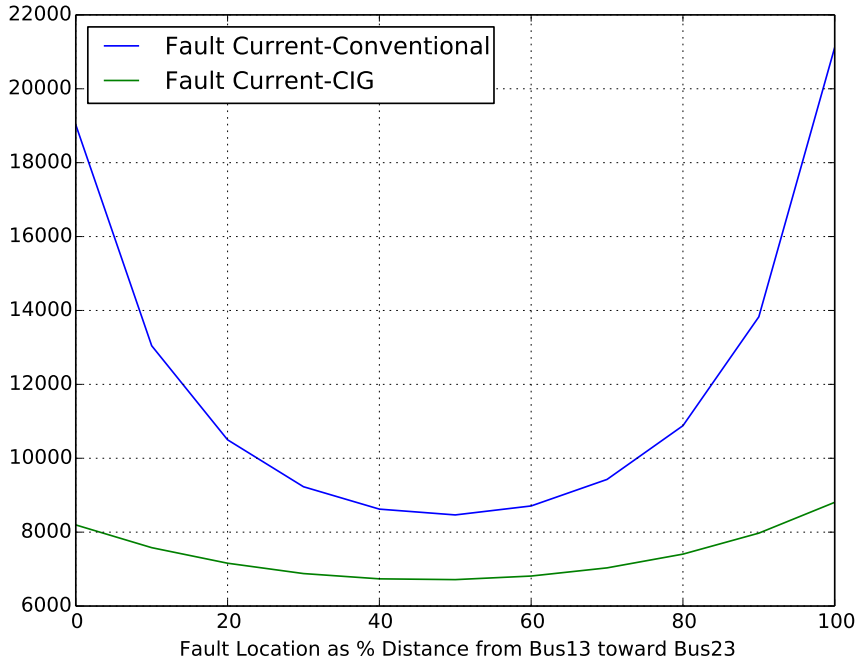

Figure 46: Fault currents from Bus 13 toward Bus 23

As the fault progresses from a source toward another source, the difference in fault currents is minimum near the middle of the line and maximum near the ends of the line.

CHAPTER 5

MITIGATIONS

To assess the ability to mitigate the observed frequency and voltage response issues, active power injection and reactive power injection models were created. The combination of active and reactive power injections can represent the capabilities of energy storage systems, or special control modes available for modern CIG equipment.

The reactive power injection was modeled as a static var compenstator (SVC), which is designed to maintain the terminal bus voltage at a specific level. Any disturbance which causes a voltage deviation at the terminal bus of the SVC will trigger reactive power injection or absorption. SVC models rated at 50MVAR were placed at bus 5 and bus 19 in the 100% CIG case.

The active power injection was modeled as two constant power loads of equal magnitude and opposite polarity, attached to the same bus. While both loads are connected to the system, they effectively cancel each other. At the point of desired injection, the positive load is switched out, with the result being an active power injection equal in magnitude to the negative load. In order to halt the power injection, the positive load is reconnected to the system. An active power injection model rated at 200MW was placed at bus 5 in the 100% CIG case.

Using the 100% CIG system, active and reactive power injection mitigations were simulated for the base set of disturbances. With a 13 cycle duration active power injection of 200MW initiated 2 cycles into the fault, the average system frequency nadir was increased by about 0.65Hz. Maintaining active power margins in CIG equipment requires underutilization of available energy, but this may allow for frequency response.

It is evident that active power is capable of reaching farther in the system from its source than reactive power. Transmission system active power losses are relatively small, when compared to transmission system reactive power losses. Therefore, active power injections for disturbance mitigation may be relatively distant from a disturbance and remain effective. Reactive power injections, though, must be closer to the disturbance to remain effective. Therefore, the effect of the SVCs during a disturbance was to regulate the voltages near their respective buses. The effect of the active power injection during a disturbance was to arrest the frequency decline for most of the system.

Figure 47 shows the CIG system frequency response to a short power injection initiated in response to the fault. the active power injection was initiated 2 cycles into the fault and lasted for a duration of 13 cycles. It is clear that the power injection restrained the frequency dip to about one-half of the deviation without power injection.

Figure 48 shows the CIG system voltage response with the described reactive compensation implemented. It is clear that the reactive power injection reduced the severity of voltage oscillations local to the reactive injection point.

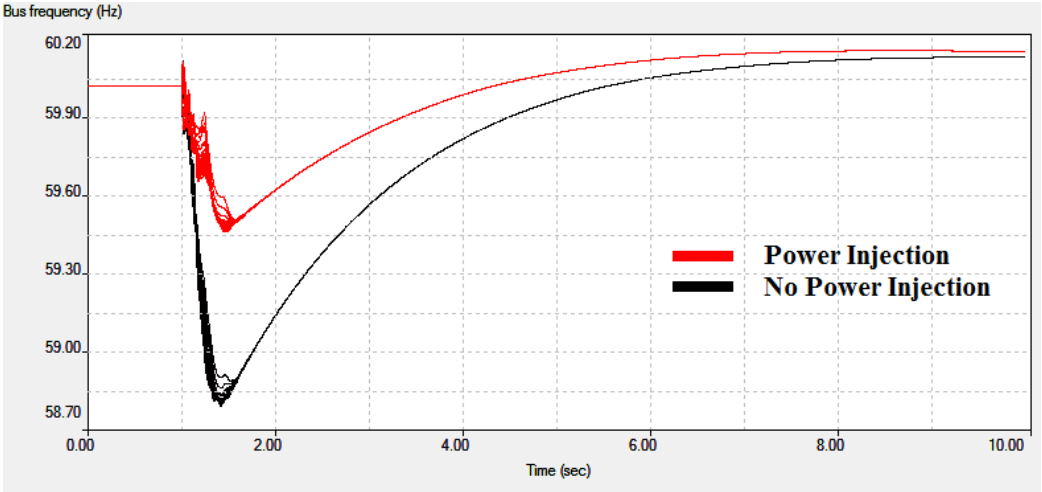

Figure 47: System bus frequency response for 100% CIG case with and without active power injection.

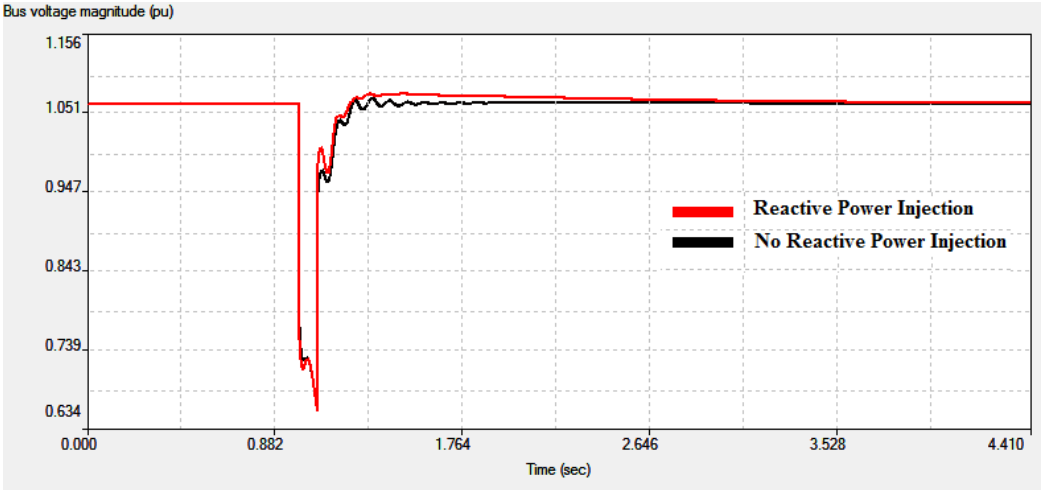

Figure 48: Bus6 voltage response for 100% CIG case with and without reactive power injection.

CHAPTER 6

CONCLUSIONS AND FUTURE WORK

The RTS 24 Bus power system model has been modified to accommodate dynamic and fault analysis. A comprehensive set of simulations has been performed to assess the impact of increased penetration of converter interfaced generation. The simulation and analysis revealed that increased penetration of converter interfaced generation into a conventional power system changes the characteristics of the system with regard to dynamic stability and fault current magnitudes. Increased magnitudes of frequency deviation and decreased fault current magnitudes have been observed as a result of displacement of conventional generation by CIG. Active power injection into the system in response to disturbances has been shown to arrest frequency decline, thereby compensating for some inertia displacement. Therefore, maintaining active power margins in CIG equipment or implementing energy storage may provide flexibility to the system and improve the system response to disturbances, although no indication is made that such things are an absolute requirement.

Power electronic converter ratings limit the fault current contribution from CIG sources to values much lower than conventional generators. The network impedance can reduce the impact of these converter limitations on fault current levels at remote buses, even though the local buses may see a dramatic decrease in fault current levels. As penetration of CIG into power systems increases, fault current levels may begin to approach load current levels. This condition may require new protection methods to maintain reliable and secure protection as power systems evolve.

6.1 Future Work

The models used for CIG were developed to replicate the terminal behavior of specific wind generator technology, as seen in mostly conventional power systems. Therefore, it is possible that this terminal behavior will become less accurate as the power system changes dramatically, as demonstrated in this research. Investigation of the system behavior using detailed models of CIG equipment would address some of the deficiencies of this research.

The dynamic stability simulation tools available only consider positive sequence networks for the solution of disturbances. This means that simulation of unbalanced disturbances, such as 1LG and L-L faults, are not accurately represented away from the fault itself in dynamic simulations. Investigation using full three-phase models of the power system and CIG equipment in an electromagnetic transients program would help address some of these deficiencies. This type of study could also indicate the effects of high frequency transients in the system as a result of CIG.

The results of this research indicate that an investigation of the protective relaying requirements in a CIG system will be very important. Since many of the existing power system protection techniques rely on fault currents that are much larger than load currents, new techniques may be required as fault currents become nearly indistinguishable from load currents. Furthermore, the variance in dispatch of renewable generation can make calculation of robust protective relay settings difficult.

Power electronic converters have minimum voltage thresholds, below which the converter will not allow switching of the power electronic components. Therefore, faults very near the converter may temporarily eliminate any fault contribution by the converter. Investigation using accurate models of converter protection and control functions in an electromagnetic transients program may provide a better understanding of system behavior for faults very near power electronic converters. Furthermore, better methods of simulation should be pursued to eliminate numerical limitations

encountered with the current limiting fault calculation method. Many different studies may be required, as there exists a large variety of power electronic technologies for renewable resource integration into the grid[27].

An in depth study of energy storage in CIG systems would provide useful information for the industry as renewable generation continues to expand worldwide. Coordinated control between various CIG in the power system, with or without energy storage, could be used to optimize system response. Due to the large variety of energy storage technologies being developed and actively researched[27], there are many potential opportunities for system improvement.

APPENDIX A

BLOCK DIAGRAMS AND PARAMETERS

Block diagrams, including parameter values, for the dynamic models used in this research are provided in this appendix. The block diagrams are referenced from the PowerWorld Simulator help files[28]. The parameter values were selected from data made available by Anderson[3], except for the power system stabilizer parameters which were generated using an optimization feature of TSAT.

Machine Model GENROU

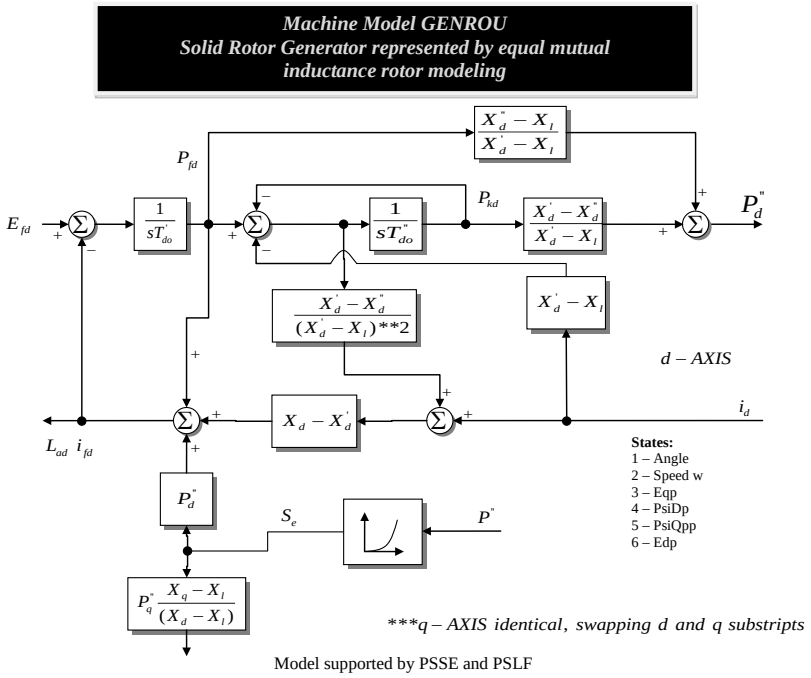

Figure 49: GENROU Block Diagram

Table 11: GENROU Model Parameters for the 24-Bus System Rotors

MVA Base	500	438	247	195	125	100	95	63	25	15
T'do	5.432	5.21	5.9	5.9	5.9	4.2	7.5	6.6	4.61	4.2
T"do	0.042	0.042	0.033	0.033	0.042	0.035	0.054	0.038	0.054	0.035
T'qo	1.5	1.5	0.535	0.54	0.3	0.792	1.5	0.792	1.5	0.792
T"qo	0.042	0.042	0.078	0.076	0.099	0.0977	0.107	0.0977	0.107	0.0977
H	3.704	2.621	3.302	3.963	4.985	2.611	11.4	5.078	8.877	2.611
D	0	0	0	0	0	0	0	0	0	0
Xd	1.7668	1.798	1.651	1.7	1.18	0.911	1.64	1.27	1.85	0.911
Xq	1.7469	1.778	1.59	1.64	1.05	0.58	1.575	1.24	1.74	0.58
X'd	0.2738	0.324	0.232	0.245	0.22	0.408	0.159	0.209	0.225	0.408
X'q	1.0104	1.051	0.38	0.38	0.38	0.58	0.306	0.85	0.4	0.58
X"d	0.2284	0.26	0.171	0.185	0.145	0.329	0.102	0.105	0.155	0.329
Xl	0.1834	0.193	0.102	0.11	0.075	0.2	0.113	0.108	0.113	0.2
S(1.0)	0.2632	0.162	0.105	0.1251	0.0933	0.16	0.087	0.2067	0.11	0.16
S(1.2)	0.5351	0.508	0.477	0.7419	0.4044	0.446	0.2681	0.724	0.42	0.446

Exciter ESAC1A

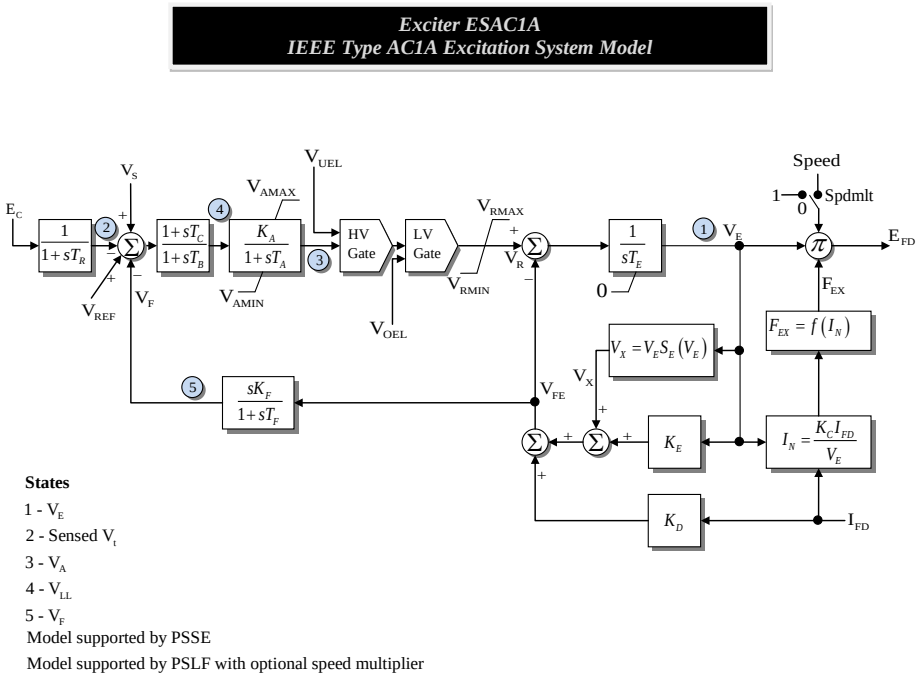

Figure 50: ESC1A Block Diagram

Table 12: ESAC1A Model Parameters for the 24-Bus System Excitation Systems

MVA Base	500	438	247	195	125	100	95	63	25	15
TR	0	0	0	0	0	0	0	0	0	0
TB	0	0	0	0	0	0	0	0	0	0
TC	0	0	0	0	0	0	0	0	0	0
KA	400	400	400	400	400	400	400	400	400	400
TA	0.02	0.02	0.02	0.02	0.02	0.02	0.02	0.02	0.02	0.02
VAMAX	14.5	14.5	14.5	14.5	14.5	14.5	14.5	14.5	14.5	14.5
VAMIN	-14.5	-14.5	-14.5	-14.5	-14.5	-14.5	-14.5	-14.5	-14.5	-14.5
TE	0.8	0.8	0.8	0.8	0.8	0.8	0.8	0.8	0.8	0.8
KF	0.03	0.03	0.03	0.03	0.03	0.03	0.03	0.03	0.03	0.03
TF	1	1	1	1	1	1	1	1	1	1
KC	0.2	0.2	0.2	0.2	0.2	0.2	0.2	0.2	0.2	0.2
KD	0.38	0.38	0.38	0.38	0.38	0.38	0.38	0.38	0.38	0.38
KE	1	1	1	1	1	1	1	1	1	1
E1	4.18	4.18	4.18	4.18	4.18	4.18	4.18	4.18	4.18	4.18
SE(E1)	0.1	0.1	0.1	0.1	0.1	0.1	0.1	0.1	0.1	0.1
E2	3.14	3.14	3.14	3.14	3.14	3.14	3.14	3.14	3.14	3.14
SE(E2)	0.03	0.03	0.03	0.03	0.03	0.03	0.03	0.03	0.03	0.03
VRMAX	6.03	6.03	6.03	6.03	6.03	6.03	6.03	6.03	6.03	6.03
VRMIN	-5.43	-5.43	-5.43	-5.43	-5.43	-5.43	-5.43	-5.43	-5.43	-5.43

Governor IEESGO

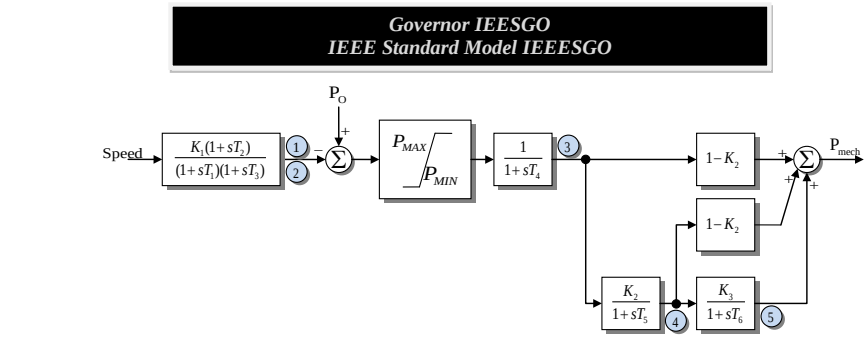

States

1 - First Integrator
2 - Second Integrator
3 - Turbine T4
4 - Turbine T5
5 - Turbine T6

Model supported by PSSE

Figure 51: IEESGO Block Diagram

Table 13: IEESGO Model Parameters for the 24-Bus System Governor Systems

MVA Base	500	438	247	195	125	100	95	63	25	15
T1	0.18	0.22	0.083	65.3	0.09	48.44	0.5	0.2	0	48.44
T2	0	0	0	6.2	0	4.634	1.25	0	0	4.634
T3	0.04	0.2	0.2	0.5	0.2	0.1	0.7	0.3	0.1	0.1
T4	0.25	0.25	0.05	0	0	0	0.7	0.09	0	0
T5	8	8	8	0.65	0	0.579	0	0	0.1	0.579
T6	0	0	0	0	0	0	0	0	0	0
K1	20	20	20	26.32	20	20	25	12.82	20	20
K2	0	0	0	0	0	0	0	0	0	0
K3	0	0	0	0	0	0	0	0	0	0
PMAX	1	1	1	1	1	1	1	1	1	1
PMIN	0	0	0	0	0	0	0	0	0	0
Pgen (Powerflow)	363.52	70.5	179.03	140.86	90.88	10.91	69.07	45.44	18.18	10.91
Pmax (Powerflow)	400	350	197	155	100	12	76	50	20	12

Stabilizer PSS2A

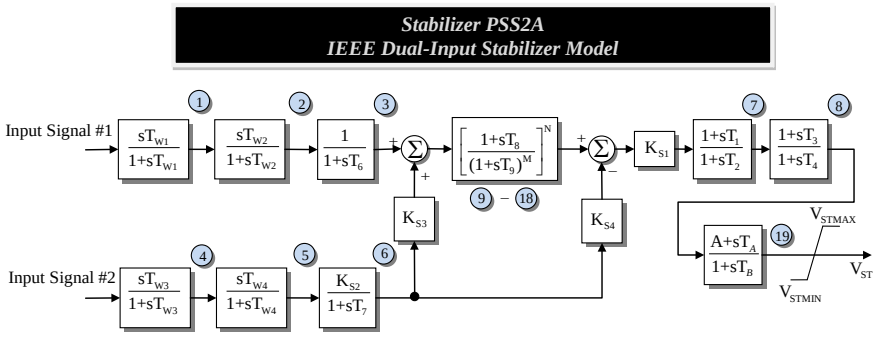

States

1 - WOTW1 11 - RampFilter3
2 - WOTW2 12 - RampFilter4
3 - Transducer1 13 - RampFilter5
4 - WOTW3 14 - RampFilter6
5 - WOTW4 15 - RampFilter7
6 - Transducer2 16 - RampFilter8
7 - LL1 17 - RampFilter9
8 - LL2 18 - RampFilter10
9 - RampFilter1 19 - LLGEOnly
10 - RampFilter2

Model supported by PSLF

Model supported by PSSE without T_A,T_B lead/lag block and with $K_{S4} = 1$

Figure 52: PSS2A Block Diagram

Table 14: PSS2A Model Parameters for the 24-Bus System Power System Stabilizers

MVA Base	500	438	247	195	125	100	95	63	25	15
ICS1	1	1	1	1	1	1	1	1	1	1
REMBUS1	0	0	0	0	0	0	0	0	0	0
ICS2	3	3	3	3	3	3	3	3	3	3
REMBUS2	0	0	0	0	0	0	0	0	0	0
M	5	5	5	5	5	5	5	5	5	5
N	1	1	1	1	1	1	1	1	1	1
Tw1	2	2	2	2	2	2	2	2	2	2
Tw2	2	2	2	2	2	2	2	2	2	2
T6	0	0	0	0	0	0	0	0	0	0
Tw3	2	2	2	2	2	2	2	2	2	2
Tw4	0	0	0	0	0	0	0	0	0	0
T7	2	2	2	2	2	2	2	2	2	2
KS2	0.27	0.3815	0.3028	0.3148	0.2006	0.383	0.0877	0.1969	0.1127	0.383
KS3	1	1	1	1	1	1	1	1	1	1
T8	0.5	0.5	0.5	0.5	0.5	0.5	0.5	0.5	0.5	0.5
T9	0.1	0.1	0.1	0.1	0.1	0.1	0.1	0.1	0.1	0.1
KS1	15.05	15.05	18.1	15.05	11.6	15.05	15.05	6.6	15.05	11.6
T1	0.124	0.145	0.178	0.152	0.198	0.191	0.211	0.226	0.18	0.19
T2	0.01	0.01	0.013	0.011	0.014	0.014	0.015	0.016	0.013	0.014
T3	0.124	0.145	0.178	0.152	0.198	0.191	0.211	0.226	0.18	0.19
T4	0.01	0.01	0.013	0.011	0.014	0.014	0.015	0.016	0.013	0.014
VSTMAX	0.1	0.1	0.1	0.1	0.1	0.1	0.1	0.1	0.1	0.1
VSTMIN	-0.1	-0.1	-0.1	-0.1	-0.1	-0.1	-0.1	-0.1	-0.1	-0.1

Exciter WT4E1

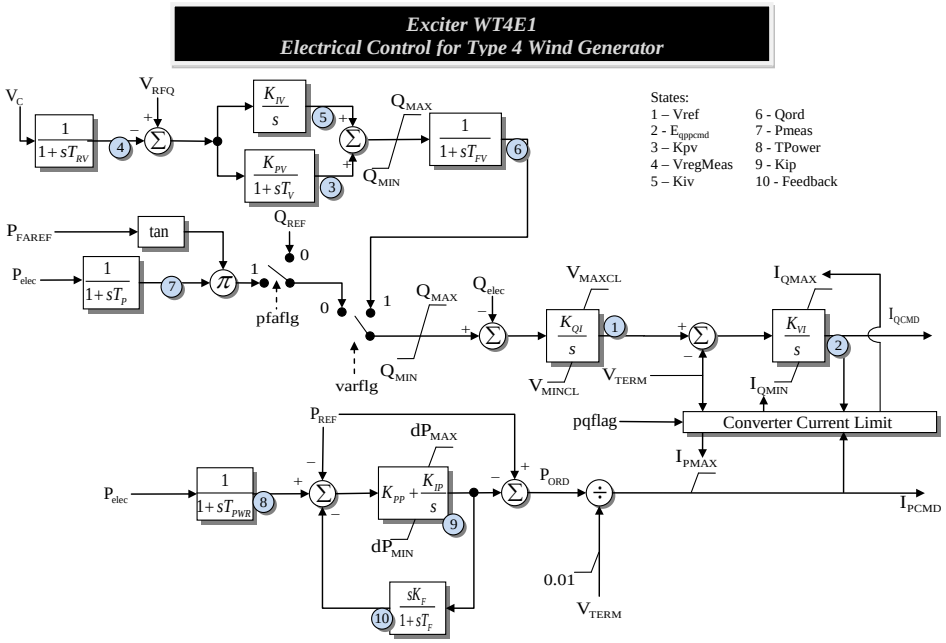

Model supported by PSSE

Figure 53: WT4E1 Block Diagram

Machine Model WT4G1

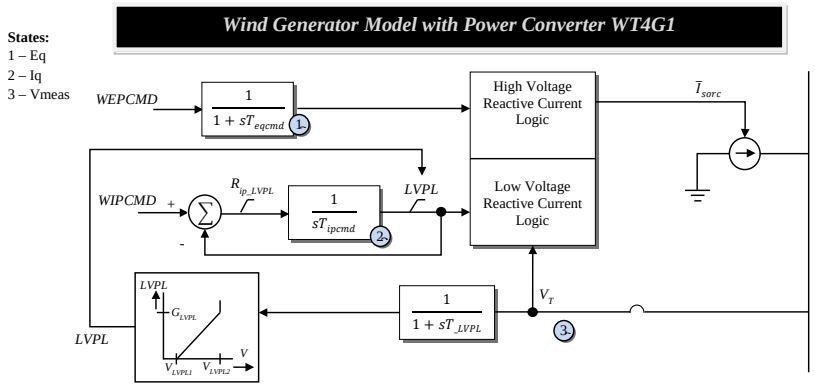

Model supported by PSEE

Figure 54: WT4G1 Block Diagram

APPENDIX B

POWER FLOW SOLUTION SCRIPT

The following python script was developed and used to solve the power flow problem for the simple system depicted in Figure 1 using the Newton/Rhapson method.

```
## newton/rhapson power flow solution for simple system
# import symbolic toolbox
from sympy import *

# define symbolic variables
v2,d2,d3 = symbols ('v2 d2 d3')

# define admittance matrix
Y11=(0.173310235142708-4.15944528579712j)
Y12=(-0.173310235142708+4.15944528579712j)
Y13=(0+0j)

Y21=(-0.173310235142708+4.15944528579712j)
Y22=(0.198309611529112-9.15932035446167j)
Y23=(-0.024999376386404+4.99987506866455j)

Y31=(0+0j)
Y32=(-0.024999376386404+4.99987506866455j)
Y33=(0.024999376386404-4.99987506866455j)

Y = Matrix([
    [Y11,Y12,Y13],
    [Y21,Y22,Y23],
```

```
    [Y31,Y32,Y33]
    ])

# define power flow equations
p2 = v2**2*Y22.real + v2*(Y21.real*cos(d2) + Y21.imag*sin(d2)) + v2*(Y23
    .real*cos(d2-d3) + Y23.imag*sin(d2-d3)) + 2.05
p3 = Y33.real + v2*(Y32.real*cos(d3-d2) + Y32.imag*sin(d3-d2)) - 0.25
q2 = -v2**2*Y22.imag + v2*(Y21.real*sin(d2) - Y21.imag*cos(d2)) + v2*(
    Y23.real*sin(d2-d3) - Y23.imag*cos(d2-d3)) - 1 + 0.5125

# determine partial derivatives
dp2_d2 = diff(p2,d2)
dp2_d3 = diff(p2,d3)
dp2_v2 = diff(p2,v2)

dp3_d2 = diff(p3,d2)
dp3_d3 = diff(p3,d3)
dp3_v2 = diff(p3,v2)

dq2_d2 = diff(q2,d2)
dq2_d3 = diff(q2,d3)
dq2_v2 = diff(q2,v2)

# define equations matrix
G = Matrix([
    [p2],
    [p3],
    [q2]
    ])

# define jacobian
J = Matrix([
```

```
    [dp2_d2,dp2_d3,dp2_v2],
    [dp3_d2,dp3_d3,dp3_v2],
    [dq2_d2,dq2_d3,dq2_v2]
    ])

# function to evaluate numerical jacobian
def Jn(d2n,d3n,v2n):
    a = J.subs(v2,v2n)
    b = a.subs(d2,d2n)
    c = b.subs(d3,d3n)
    return c

# function to evaluate numerical equations
def Gn(d2n,d3n,v2n):
    a = G.subs(v2,v2n)
    b = a.subs(d2,d2n)
    c = b.subs(d3,d3n)
    return c

def degrees(x):
    return N(x*180/pi)

# flat start initial guess
estimate = Matrix([
    [0],
    [0],
    [1]
    ])

# initial error
error = N(Jn(0,0,1)**-1*Gn(0,0,1))
```

```
# iterate solution using newton/rhapson method
for x in range(11):
    # print iteration results
    print x,';',list([N(degrees(estimate[0]),4),N(degrees(estimate[1])
        ,4),N(estimate[2],4)]),';',list(N(Gn(estimate[0],estimate[1],
        estimate[2]),2))
    # adjust estimate by error
    t = estimate
    estimate = estimate - error
    # update jacobian and error estimate
    error = N(Jn(estimate[0],estimate[1],estimate[2])**-1*Gn(estimate
        [0],estimate[1],estimate[2]))
```

REFERENCES

[1] Thomas Ackermann, editor. *Wind Power in Power Systems*. John Wiley and Sons, Ltd, second edition, 2012.

[2] Arthur R. Bergen and Vijay Vittal. *Power Systems Analysis*. Prentice-Hall, Inc., second edition, 2000.

[3] P.M. Anderson. *Power System Control and Stability*. John Wiley and Sons, Inc, second edition, 1994.

[4] P.M. Anderson. *Analysis of Faulted Power Systems*. John Wiley and Sons, Inc, 1995.

[5] J. Lewis Blackburn. *Symmetrical Components for Power Systems Engineering*. Marcel Dekker, Inc, 1993.

[6] John J. Grainger and Jr. William D. Stevenson. *Power System Analysis*. McGraw-Hill, Inc, 1994.

[7] Prabha Kundur. *Power System Stability and Control*. McGraw-Hill, Inc, 1994.

[8] Carson W. Taylor. *Power System Voltage Stability*. McGraw-Hill, Inc, 1994.

[9] P. Kundur, J. Paserba, V. Ajjarapu, G. Andersson, A. Bose, C. Canizares, N. Hatziargyriou, D. Hill, A. Stankovic, C. Taylor, T. Van Cutsem, and V. Vittal. Definition and classification of power system stability ieee/cigre joint task force on stability terms and definitions. *Power Systems, IEEE Transactions on*, 19(3):1387–1401, Aug 2004.

[10] Joseph H. Eto, John Undrill, Peter Mackin, Ron Daschmans, Ben Williams, Brian Haney, Randall Hunt, Jeff Ellis, Howard Illian, Carlos Martinez, Mark O'Malley, Katie Coughlin, and Kristina Hamachi LaCommare. Use of frequency response metrics to assess the planning and operating requirements for reliable integration of variable renewable generation. Technical Report LBNL-4142E, Ernest Orlando Lawrence Berkeley National Laboratory, December 2010.

[11] M.P. Kazmierkowski and L. Malesani. Current control techniques for three-phase voltage-source pwm converters: a survey. *Industrial Electronics, IEEE Transactions on*, 45(5):691–703, Oct 1998.

[12] J. Holtz. Pulsewidth modulation for electronic power conversion. *Proceedings of the IEEE*, 82(8):1194–1214, Aug 1994.

[13] Eknath Vittal. *The Impact of Reactive Power From Wind Generation on Power System Stability*. PhD dissertation, University College Dublin, School of Electrical, Electronic & Mechanical Engineering, September 2011.

[14] E. Camm and C. Edwards. Reactive compensation systems for large wind farms. In *Transmission and Distribution Conference and Exposition, 2008. T x00026;D. IEEE/PES*, pages 1–5, April 2008.

[15] I.S. Naser, O. Anaya-Lara, and K.L. Lo. Study of the impact of wind generation on voltage stability in transmission networks. In *Electric Utility Deregulation and Restructuring and Power Technologies (DRPT), 2011 4th International Conference on*, pages 39–44, July 2011.

[16] E. Vittal, M. O'Malley, and A. Keane. Rotor angle stability with high penetrations of wind generation. *Power Systems, IEEE Transactions on*, 27(1):353–362, Feb 2012.

[17] E. Vittal, M. O'Malley, and A. Keane. A steady-state voltage stability analysis of power systems with high penetrations of wind. *Power Systems, IEEE Transactions on*, 25(1):433–442, Feb 2010.

[18] L. Meegahapola and D. Flynn. Impact on transient and frequency stability for a power system at very high wind penetration. In *Power and Energy Society General Meeting, 2010 IEEE*, pages 1–8, July 2010.

[19] Yanhua Liu, Yongning Chi, Weisheng Wang, and Huizhu Dai. Impacts of large scale wind power integration on power system. In *Electric Utility Deregulation and Restructuring and Power Technologies (DRPT), 2011 4th International Conference on*, pages 1301–1305, July 2011.

[20] C. Rahmann, H.-J. Haubrich, A. Moser, R. Palma-Behnke, L. Vargas, and M.B.C. Salles. Justified fault-ride-through requirements for wind turbines in power systems. *Power Systems, IEEE Transactions on*, 26(3):1555–1563, Aug 2011.

[21] S. Alepuz, S. Busquets, J. Bordonau, J. Pontt, C. Silva, and J. Rodriguez. Comparison of control strategies to meet low voltage ride-through requirements in distributed power generation systems. In *Industrial Electronics, 2007. ISIE 2007. IEEE International Symposium on*, pages 2619–2624, June 2007.

[22] Wei Qiao and R.G. Harley. Effect of grid-connected dfig wind turbines on power system transient stability. In *Power and Energy Society General Meeting - Conversion and Delivery of Electrical Energy in the 21st Century, 2008 IEEE*, pages 1–7, July 2008.

[23] Lidong Zhang, Lennart Harnefors, and H.-P. Nee. Power-synchronization control of grid-connected voltage-source converters. *Power Systems, IEEE Transactions on*, 25(2):809–820, May 2010.

[24] P.M. Subcommittee. Ieee reliability test system. *Power Apparatus and Systems, IEEE Transactions on*, PAS-98(6):2047–2054, Nov 1979.

[25] E. Muljadi, N. Samaan, V. Gevorgian, Jun Li, and S. Pasupulati. Short circuit current contribution for different wind turbine generator types. In *Power and Energy Society General Meeting, 2010 IEEE*, pages 1–8, July 2010.

[26] P. Pourbeik. Generic models and model validation for wind and solar pv generation: Technical update. Technical Report 1021763, Electric Power Research Institute, December 2011.

[27] J.M. Carrasco, L.G. Franquelo, J.T. Bialasiewicz, E. Galvan, R.C.P. Guisado, Ma.A.M. Prats, J.I. Leon, and N. Moreno-Alfonso. Power-electronic systems for the grid integration of renewable energy sources: A survey. *Industrial Electronics, IEEE Transactions on*, 53(4):1002–1016, June 2006.

[28] PowerWorld. Block diagrams for powerworld simulator simulations, 2014. [Online; accessed 16-November-2014].